Modelling the Flow Induced Evolution of Ice Fabric

-A Study of Ice Cores from Central Greenland

Master Thesis

by Asbjørn Persson

Supervisor: Dorthe Dahl-Jensen

Niels Bohr Institute

Ice and Climate

University of Copenhagen

May 31, 2006

Abstract

Polycrystalline ice undergoing deformation by intracrystalline slip develops a preferred orientation of c-axes (fabric), leading to anisotropic flow properties of the polycrystal. Implementations of Azuma's and Sachs' flow laws are coupled with two models for flow induced lattice rotations, Lister's model and the Schmid-Boas model. The models are compared with observed fabric from the Greenland GRIP and NorthGRIP ice cores, using the Dansgaard-Johnsen model. Studies of other dry-zone ice cores finds a degree of orientation, $R \sim 0.3$ near the surface, although the GRIP measurements suggest a somewhat lower value. Assuming an initial value of $R = 0.30$ at GRIP, it is found that the models overestimate the lattice rotations of grains by $\sim 185\%$ compared to observations. A correction to the Schmid-Boas model reducing the lattice rotation to 35% of the original value is proposed. This model matches the observed fabric at GRIP except in the deepest $z \sim 300\,m$, without the inclusion of recrystallization models. A simple extension of this model to a more general stress state is presented and applied on the NorthGRIP core, showing very good agreement with observations in the upper $1400\,m$.

Contents

Chapter 1

Introduction

The Greenland ice sheet is more than 3 km thick at the center, stretching 500 km from east to west and more than 2000 km from north to south. In the cold central parts of the ice sheet a net annual snow accumulation leads to a stratigraphic layering of the precipitation. As the layers sink they are gradually compressed into ice. The annual layers are gradually thinned because ice flows from the central areas towards the coastal areas, where it is removed by calving or melting. The isotopic composition of each layer is related to the surface temperature at the time of deposition [Dansgaard, 1964]. Although ice in central parts of the great ice sheets is very clean, trace quantities of soluble and insoluble impurities are present in the ice. Such impurity content of dust, ions along with trapped air reveal volcanic events and information about past atmospheric circulation and composition. The ice sheets thus form high resolution climatic archives, provided a relationship between depth and age is established. To study these data, ice cores have been drilled in glaciers all over the world, e.g. see Figure 1.1. The drilled ice cores have been dated using a combination of stratigraphic layer counting and simple ice flow models.

In the simple models, the movement of ice is determined from the criterion of

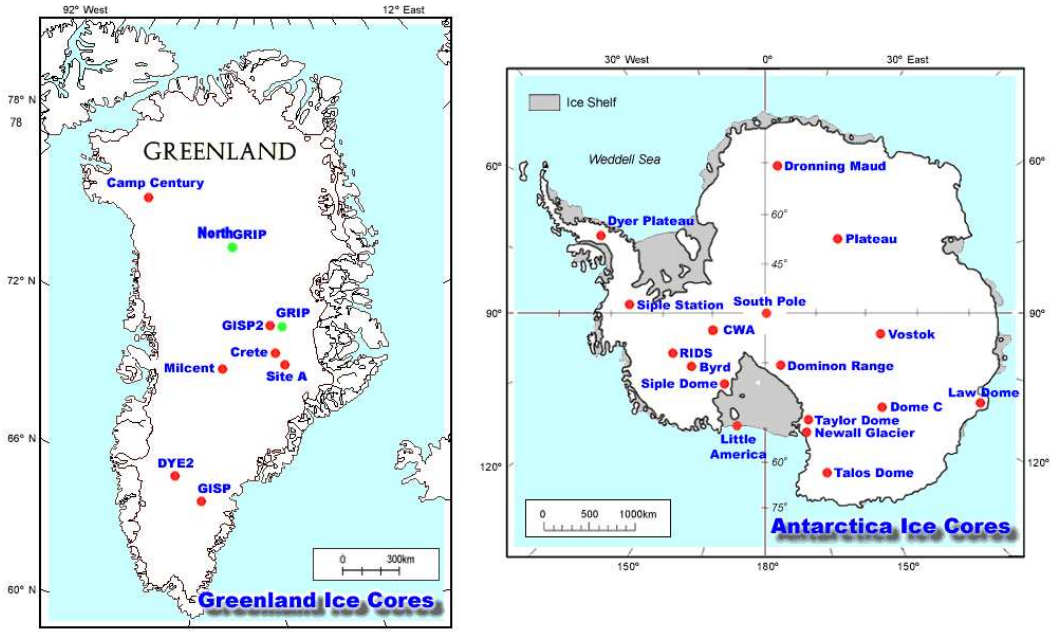

Figure 1.1: *Locations of drilled ice cores. This work will focus mainly on two deep cores from Central Greenland Ice Sheet, the GRIP and NorthGRIP cores. The* $3028.65\,m$ *long GRIP core was drilled between 1989-92 close to the present Summit of the ice sheet, at* $72^o34.5'N, 37^o38.5'W$*,* 3230 *meters above sea level [GRIP Members, 1993]. The NorthGRIP project, was initiated in 1996 reaching bedrock at depth* $3085\,m$ *in 2003. The drill site is located* $75^o6.0'N, 42^o19.2'W$*,* $316\,km$ *NNW of GRIP [Andersen et al., 2004]. Figures from http://www.nicl-smo.sr.unh.edu*

local mass balance, such that the shape of the ice sheet is constant in time. These models, e.g. the Dansgaard-Johnsen model [Dansgaard and Johnsen, 1969], have proved to be very reliable at dating annual layers in the ice sheets, mainly because the deviations from mass balance are very small compared to the velocities observed in the ice sheets. However, the ice sheets themselves are not merely keeping record of the climatic variations, they also form important feedbacks to the climate system. For instance, it has been proposed that surges of fresh water from the Laurentide ice sheet are related to millennia scale climatic oscillations, during the last stadial, known as Bond cycles [Ganopolski and Rahmstorf, 2001]. The formation of new ice sheets drastically changes the albedo and the topography of the Earth's surface. Furthermore, the ice sheets are huge reservoirs of fresh water, and changes in their volumes directly affect the sea surface level and the salinity of the oceans. Indeed, melting of the large ice sheets in Greenland and Antarctica would raise the mean global sea surface level by almost $70\,m$. In this light it is also important to model the *changes* to the ice sheets, the extent of margins and thickness.

In ice sheets, the flow of ice is driven by the curvature of the ice surface. The ice surface tends to align itself such that mass balance is achieved. Hence any change to the climatic conditions implies a change to the form of the ice sheet, until a new steady-state form is obtained. In order to investigate the time evolution of ice sheets a relation between the stress and deformation, a constitutive relation, must be applied. In 1955 Glen proposed such a relation for ice, namely Glen's law [Glen, 1955]. Glen's law has been used with great success in modelling the flow and shapes of ice sheets. Glen's law, however, contains limitations.

Flowing ice develops strongly anisotropic rheological properties, related to the microstructure of the ice. Glen's law cannot account for this anisotropy. Deep in the ice cores large discrepancies to observations have been reported. More

complicated flow models, e.g. Sachs' model [Sachs, 1928] and Azuma's model [Azuma, 1994], take the anisotropy into account and quantifies its evolution with flow. Potentially these models could provide significant improvements to Glen's law; however, they are limited in being computationally intensive and their ability to correctly determine the evolution of anisotropy is not properly tested. Although extensive laboratory studies of the flow induced evolution of the microstructure of ice have been performed, the high stresses applied in these experiments, make it difficult to compare the results to the real flow in ice sheets. Instead the ice cores provide a unique possibility to test the models against the observations of the microstructure.

This work presents a comparison between the developed microstructure, as modelled by Azuma's model and Sachs' model, and observations from the two Central Greenland cores, GRIP and NorthGRIP. Furthermore a modification to Azuma's model is proposed and tested.

1.1 Synopsis

In **Chapter 2** the microstructure of ice and the principles of ice deformation are described. Relevant observations from the GRIP and NorthGRIP ice cores are presented, and their interpretations in terms of processes affecting the microstructure of ice are discussed.

Chapter 3 describes various flow models for ice, with a main focus on Azuma's anisotropic model. The Dansgaard-Johnsen model is also described in detail.

Chapter 4 contains tests of selected anisotropic models against observations from GRIP. A modification to Azuma's model is proposed and tested against the observed microstructure at NorthGRIP

Chapter 5 provides a summary of previous discussions and results. On this basis, conclusions are made regarding the model's ability to reproduce the changing

anisotropy of flowing ice.

Chapter 2

Background and Observations

In this chapter the microstructure of ice is described, along with a brief outline of the empirical methods available to investigate it. The main focus is on the presentation of the observations performed on ice from the GRIP and NorthGRIP ice cores, from central Greenland, and a discussion of the interpretations of them.

2.1 Structure of Ice

Ice is the solid state of water (H_2O). In natural ice, I_h, the two hydrogen atoms in each water molecule remain covalently bonded with the oxygen, and each molecule forms hydrogen bonds with its four nearest neighbors at the corners of a regular tetrahedron. Thereby the oxygen atoms arrange themselves in layers of hexagonal rings with 3 bonds inside the layer and one to an adjacent layer. The layers are separated by the a distance of $0.276nm$, and termed the *basal planes*. In the basal planes, the molecules are shifted in two planes lying only $0.0923nm$ apart see Figure 2.1 (paragraph based on Pentrenko (1999)).

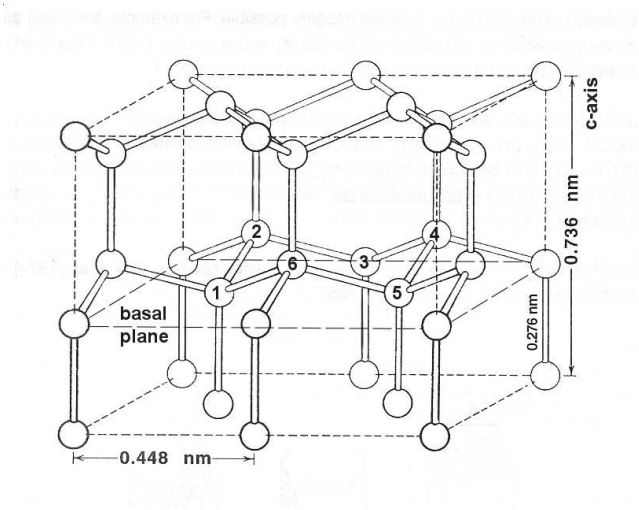

Figure 2.1: *The crystal structure of I_h. Only oxygen atoms are shown; one hydrogen atom is situated at each hydrogen bond close to either oxygen atom, such that each oxygen atom has two close hydrogen atoms. Three basal planes are shown; each layer is made of hexagonal rings, e.g. oxygen 1,2,3,4,5,6 constitute such a ring. The plane of 1,3,5 is slightly shifted compared to that of 2,4,6. Each oxygen atom forms only one inter-layer hydrogen bond. Figure modified from [Thorsteinsson, 1996]*

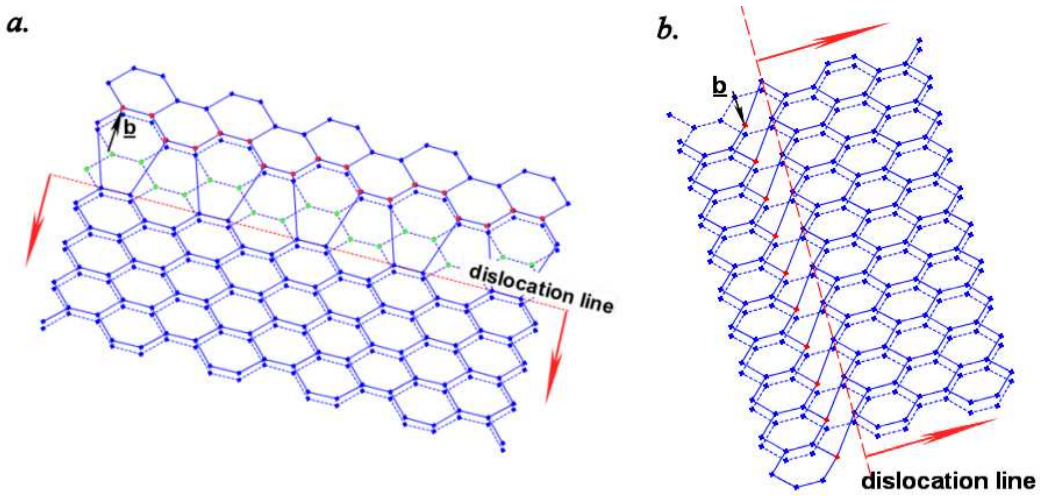

Figure 2.2: *Linear defects. Both figures show two neighboring basal planes at the plane of the fault.* **a***: An edge dislocation, in which the red atoms in the upper plane, above the dislocation line, have been displaced* **b** *relative to the lower plane, breaking a bond with every other green oxygen.* **b***: A screw dislocation, in which the red oxygen atoms have been displaced along the dislocation line. The progressive movement of either dislocation line along the arrows will shear the crystal. In reality dislocation are rarely linear, being a combination of edge and screw dislocations instead.*

2.1.1 Dislocations and Intracrystalline Slip

Imperfections in the ideal lattice structure described in Section 2.1 are divided into *Point defects* and *Linear defects*.

Point defects can be subdivided into protonic molecular and impurity defects (and more). A protonic defect is a displacement of a proton either along an O-O line or between different O-O lines. The migration of protonic defects explains the electrical conductivity of ice. Molecular defects are vacancies in or extra O-atoms inserted in the crystal lattice. Ice can deform by *diffusion creep*, which is diffusion of vacancies and extra atoms along the compressive and extensive axes respectively, see [Thorsteinsson, 1996, Petrenko and Whitworth, 1999]. In ice sheets, this deformation mode is not of primary importance [Duval et al., 1983] and it is not included in the model presented in Chapter 4.

Linear defects are defects between two neighboring planes, e.g. basal planes. The dislocated atoms lie along a line, the *displacement line*, and include *edge* dislocations and *screw* dislocations shown in Figure 2.2. For edge and screw dislocations, atoms are displaced one interatomic distance, respectively normal to or along the dislocation line and within the glide plane. The vector of displacement is known as the Burger vector, **b**. When shear stress is applied on a glide plane, ice can deform by the successive movement of existing linear defects or the formation of new ones, effectively sliding one glide plane over another. This process is known as dislocation glide. Dislocation glide on the basal plane is the most important mode of deformation in polycrystalline ice [Duval et al., 1983], although other slip systems exist. The dislocation density is the total length of dislocation line pr. unit volume. Even strain free crystals have dislocations, but

dislocation density increases with strain and temperature, in turn leading to a higher elastic energy in the grain.

2.1.2 Formation of Polycrystalline Ice

In ice sheets, ice is an aggregate of many small crystals (*grains*). New snow has a high content of air as individual snow crystals form complex patterns typically having a density $\sim 100\,kg\,m^{-3}$. The density of the snow is gradually increased through packing and diffusive processes, enhanced by weight of newer precipitation. One year after deposition the snow is often referred to as *firn* and the density is typically $\sim 400\,kg\,m^{-3}$. If the surface temperature reaches the melting point in the summer, percolation by melt water may increase the density by up to a factor of two, but at GRIP and NorthGRIP melt layers are very rare. The firn is eventually compressed into ice at a typical depth of $\sim 60-100\,m$ and density $\sim 830\,kg\,m^{-3}$, when the interconnecting air passages between the grains are completely sealed and air is only present in closed bubbles. The density increases with depth as bubbles shrink under the increasing hydrostatic pressure, reaching $\sim 917\,kg\,m^{-3}$ when the air bubbles finally disappear and the air is included in the crystal lattice as *clathrate hydrate* (paragraph based on Paterson (1994)).

In unwetted ice the original randomly oriented snow crystals form seeds for larger ice crystals. At the firn-ice transition the ice is thus an aggregate of many small ice crystals with varying orientations. The distribution of the crystal orientations, the fabric, is of primary interest. It strongly impacts on the rheological properties of the polycrystal because of the strong preference for basal glide in the individual crystals. The sizes and shapes of the crystals are known as the texture. It is generally believed that flow properties are much less influenced by the ice texture than by fabric [Jacka, 1984].

2.2 Measuring Fabric and Texture

The atomic structure of ice implies the exhibition of birefringent optical properties. Ice crystals have one optical axis, the *c*-axis, which is the normal to the basal plane. This allows the determination of fabric and texture of an ice sample by the following procedure. A thin section ($\sim 0.5\,mm$) of the aggregate is placed between crossed polarizers over a (white) light source. When linearly polarized light passes a birefringent material it will generally become elliptically polarized, allowing passage of the component of the light waves oscillating perpendicular to the original polarization through the second polarizer. In the special case of light travelling parallel to the *c*-axis no change in polarization occurs and thus no light passes the second polarizer, in effect leaving the crystal dark, and the *c*-axis is said to be brought into a *position of extinction*. Other points of extinction exist, allowing measurement of the orientation of each crystal, even when the *c*-axis lies in the plane of the thin section [Langway, 1958]. Each crystal will appear as a distinct color, depending on its orientation relative to the incident light, because the refractive index of I_h is dependent of wavelength. A picture of a thin section is shown in Figure 2.3.

Traditionally the measurements of fabric outlined above have been carried out manually, using a Rigsby stage [Rigsby, 1951]. Recently, fully automated fabric analyzers have become available, which has made it possible to dramatically increase the number of measured crystals, thereby improving the statistics [Wilen et al., 2003]. The previous manual measurement of texture and fabric is

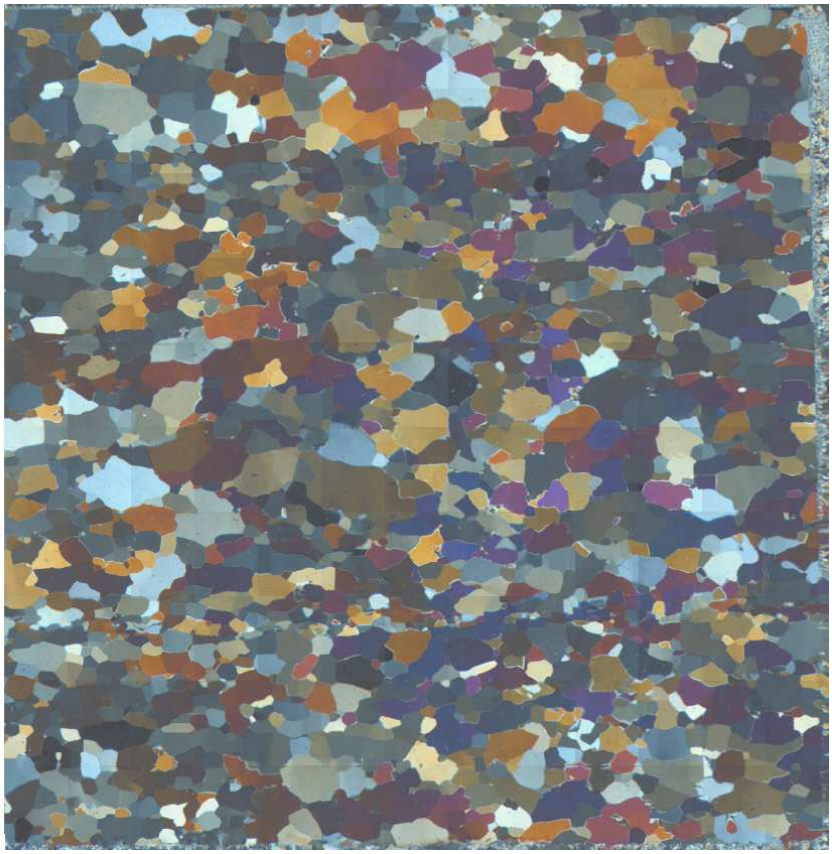

Figure 2.3: *The picture shows a vertical* $10\,cm \times 10\,cm$ *thin section from NorthGRIP, depth* $1603\,m$*, placed between crossed polaroids. Individual grains can be distinguished by color, allowing determination of crystal texture. Picture by Bizet (2006).*

a laborious task. Complete sets of measurement, from top to bottom of an ice sheet, are therefore scarce.

2.2.1 Statistical Parameters

Thin sections of ice sheet ice contain up to several thousands of grains. To compare the fabrics and textures of different thin sections some statistical parameters are required. This work will apply the following parameters: Grain size is described by the *sample mean cross sectional area* of the grains or by the *sample mean linear grain size* obtained using a linear intercept method [Thorsteinsson, 1996]. The fabric is described by the *degree of orientation*, R, [Wallbrecher, 1978] and the *eigenvalues of the cross-product tensor*, a_1, a_2, a_3 [Woodcock, 1977].

The unfamiliar reader is offered a description of these parameters in Appendix A. Graphical presentations of fabrics are also discussed here and a new continuous method of plotting orientation density is described, based on an idea by Throstur Thorsteinsson.

2.3 Ice Core Observations

Thorsteinsson et al. (1997) measured 36 thin sections along the GRIP ice core, from the Summit of the Greenland Ice sheet. The samples are roughly evenly distributed with depth, from right below the firn-ice transition to the bottom. These measurements were carried out manually, as it was before the introduction of automatic c-axis analyzers. The *degree of orientation* is presented in Figure 2.4. For reference the climatic transition is shown, denoting the transition from the previous stadial, the Wisconsin, to the present inter-stadial, the Holocene. The transition is dated to 11703 years b2k (before the year 2000AD.)

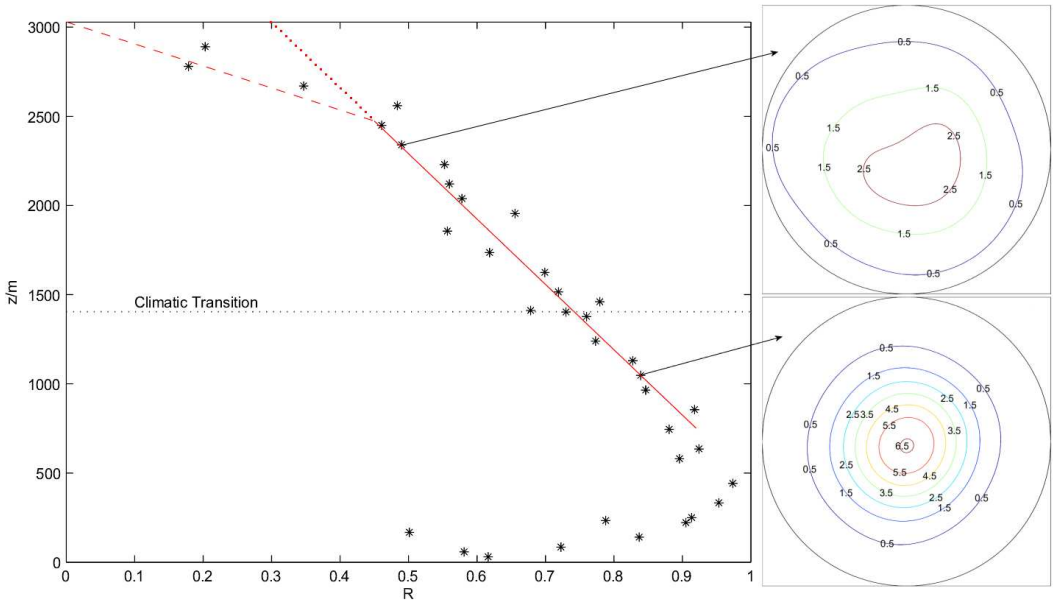

Figure 2.4: **Left***: Evolution of degree of orientation at GRIP plotted vs. height above bedrock. The asterisks show the fabric observations [Thorsteinsson et al., 1997]. The red lines show schematic interpretations of the fabric evolution, the dashed line showing the usual interpretation that fabric is isotropic near the surface and there is a kink in the evolution at the onset of the rotation recrystallization regime. The red dotted line shows an interpretation matching evolution at NorthGRIP, see text. No drastic change in fabric is observed across the transition.* **Right***: Plots of orientation density (for details, see Appendix A.2.3), at depth* $689\,m$ *and* $1982\,m$ *show examples of circular vertical fabric observed at GRIP. Units are densities relative to density of isotropic distribution.*

[Vinther et al., 2006]

The GRIP fabric is roughly circular, i.e. symmetric about the vertical axis, at all depths. The degree of orientation is seen to increase with depth towards a single maximum (vertical) fabric. In the lowest $400\,m$ the the degree orientation decreases drastically. Thorsteinsson drew the conclusion that degree of orientation at GRIP increases rapidly from almost isotropic at the firn-ice transition to about $R = 0.50$ at depth $700\,m$, then more slowly from there. This result agreed

well with later measurements on the NorthGRIP ice core drilled 316 km NNW of GRIP [Wang et al., 2002], possibly further attributing to the wide acceptance of the result. Recently however, new measurements of the upper part of the NorthGRIP core, at the Niels Bohr Institute in Copenhagen, indicated that ice at firn-ice transition was *not* isotropic and that the degree of orientation instead increased steadily from $R = 0.30$ [Svensson et al., 2003b]. Simultaneously the results of Wang et al. were corrected for a software error, which accounted for this disagreement. The corrected fabric evolution at NorthGRIP is shown in Figure 2.5.

The conclusion that the top fabric at GRIP is isotropic should be reconsidered. It seems unlikely that the transformation from snow to ice at GRIP and NorthGRIP should be radically different, as surface conditions are similar. NorthGRIP has annual ice equivalent accumulation of 0.195 m pr. year compared to 0.23 m at GRIP, while the annual mean surface temperature is -32^{o} at both sites [Andersen et al., 2004, Johnsen et al., 1992]. This view is supported by comparison with other cores. An investigation at Siple Dome near the coast of West Antarctica showed near surface fabrics very similar to those observed at NorthGRIP, even though the accumulation rate here is very different, being only 0.12 ma^{-1} ice equivalent, while the annual mean temperature is $-25^{o}C$ [Diprinzio et al., 2005]. Measurements from the interior Antarctica at Dome C show only slight initial anisotropy [Wang et al., 2003]; however, this could be related to the low mean annual surface temperature at the site of only -55^{o}. A study from Law Dome also found anisotropic fabric near the surface [Jun, 1995], although different statistics were applied in this work. A mean polar angle of $\sim 45^{o}$ was observed near surface equal to the value observed near the surface at NorthGRIP [Svensson et al., 2003b], whereas isotropic ice has a mean polar angle of 60^{o}. Furthermore, the *kink* in the fabric evolution at GRIP is entirely based on three data points, each representing only $N = 200$ crystals. Finally, a

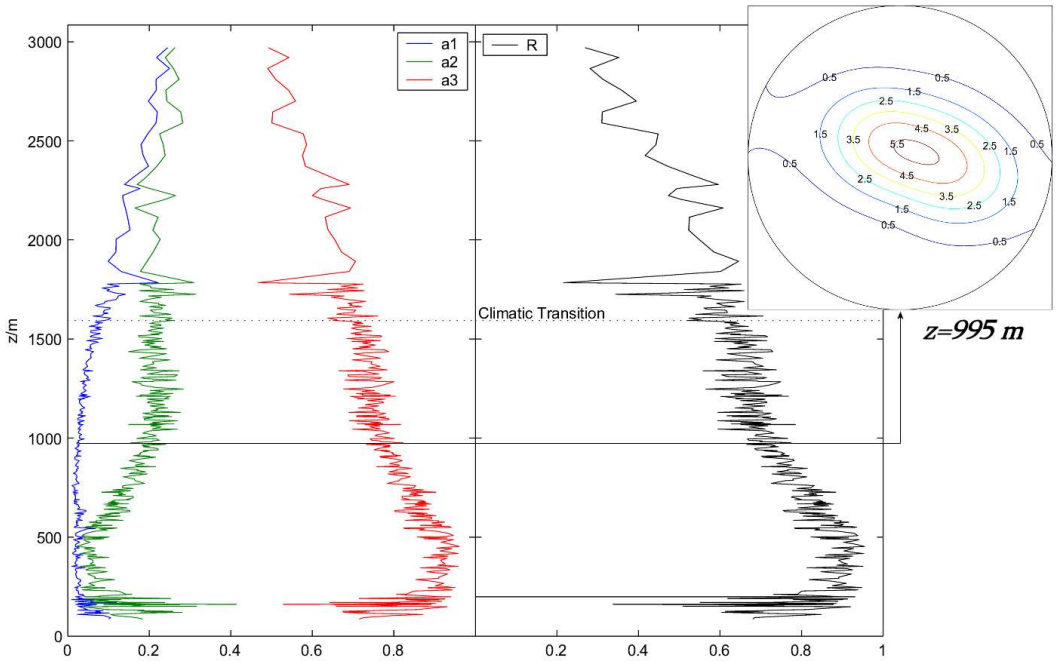

Figure 2.5: *Evolution of orientation at NorthGRIP. 365 thin sections measured by Wang et al. (2002), corrected for software error (unpublished). The vertical profile of the eigenvalues of the cross-product tensor, a_1, a_2, a_3 and the degree of orientation, R. The evolution of R and a_3 is similar to GRIP; however the fabric is* not *isotropic at the surface. A difference between a_1 and a_2 is seen to develop with depth, meaning a girdle fabric is formed. NorthGRIP is situated on an ice ridge and the girdle is generally attributed to the asymmetry of the stress field here, namely the pure shear. This will be further investigated with a flow model in Chapter 4. An example of the girdle fabric is shown to the right (Units are densities relative to density of isotropic distribution).*

study of seasonal variations in texture and fabrics, at a depth of 300 m in the NorthGRIP core, using good statistics, displayed variations in R of up to 0.15 on centimeter scale [Svensson et al., 2003a], indicating that the GRIP R-values may not be representative for the average values. On this basis, it seems likely that initial fabric at GRIP is similar to that observed at NorthGRIP, although remeasuring the fabric at GRIP will provide the only certain answer.

The mean grain diameter at GRIP increases steadily from 1.6 mm at the firn-ice transition to a limiting value around 4 mm at depth 700 m. The size is then constant with depth until the climatic transition at a depth of 1650 m, where it decreases to 2.0 mm. During the Glacial there are variations, but a slightly increasing trend in grain size is observed. At the deepest 200 m the crystal size increases dramatically. The evolution of grain size at NorthGRIP is similar. Figure 2.6 shows the evolution of grain size at GRIP and NorthGRIP.

2.4 Interpretations

The evolution of fabric and texture is a result of several processes. As ice undergoes compression, the degree of orientation will increase as the deformation of individual grains change their orientation towards the axis of compression. This process is termed the *flow induced evolution of fabric* and will be treated further in Chapter 3 and 4. The remaining part of this Chapter, describes other mechanisms influencing the microstructure of ice.

2.4.1 Recrystallization

The term *dynamic recrystallization* refers to any process that changes the texture or fabric of ice, excluding flow induced lattice rotation. It is often divided into the three processes, *normal grain growth*, *rotation recrystallization* and *migration*

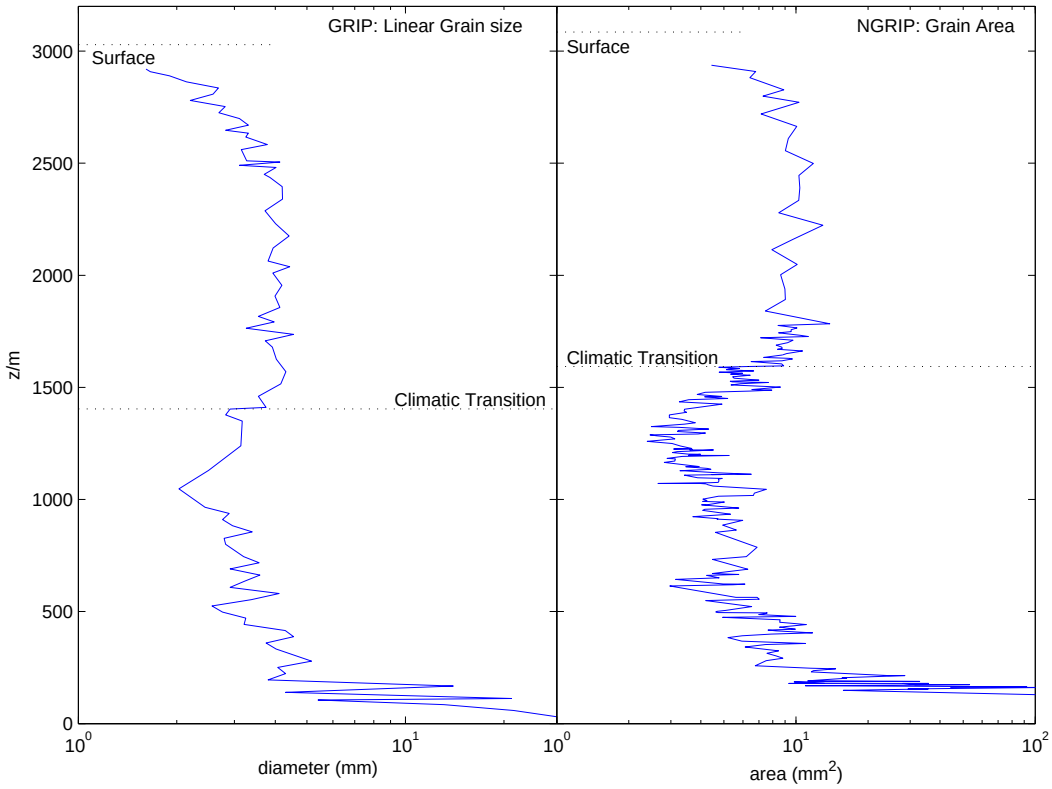

Figure 2.6: *Evolution of mean grain size as observed on the GRIP core (left) [Thorsteinsson et al., 1997] and the NorthGRIP core (right) (Wang, unpublished). Direct comparisons between the cores are difficult because of the different size measures involved. However, the general evolution of GRIP and NorthGRIP are very comparable, suggesting the influence of identical processes. Mean grain size increases from the firn ice transition stabilizing at a depth around* $700\,m$*. Grain size drastically drops below the transition, then increases again, reaching very large sizes near the bottom.*

recrystallization [Alley, 1992].

Normal Grain Growth

The grain boundaries are defects in the lattice structure of the aggregate and are associated with a certain amount of elastic energy. The free energy will thus be decreased by reducing the area of boundaries. The resulting thermodynamic force drives a reduction of boundary curvature by migration of water molecules, thereby increasing the grain sizes and removing the smallest grains. This process is known from metallurgy and predicts the following law for the temporal growth of the mean of the crystal diameters, D [Alley et al., 1986]

$$\left\langle D^2 \right\rangle = \left\langle D_0^2 \right\rangle + kt \tag{2.1}$$

where t is the time and k is a constant dependant on temperature and D_0 are the grain diameters at $t = 0$.
The elimination of strained grains, with large dislocation densities, is possibly facilitated by release of the associated energy. However, experimental studies show no relation between grain orientation and size, suggesting that normal grain growth does not affect the fabric [Svensson et al., 2003b].

In ice sheets normal grain growth is active at all depth. In the upper parts it is, however, the dominant process, explaining (although slightly overestimating) the observed grain growth at GRIP to the depth of 700 m [Thorsteinsson et al., 1997]. The increasing grain size observed in the warm deepest part of the ice sheets is probably related to the higher temperature near the bottom, as k increases with temperature.

Rotation Recrystallization

Individual grains deform mainly by basal glide, inevitably leading to a heterogenous stress distribution. Occasionally the bending moments on a grain may

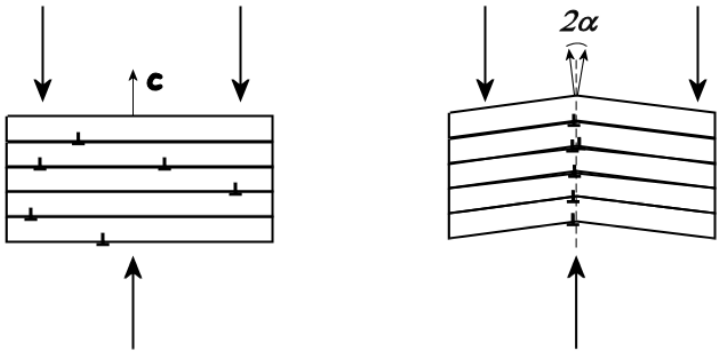

Figure 2.7: *Principle of rotation recrystallization. Heterogenous deformation implies bending moments on individual grains causing dislocations lines (marked by inverted T's) to align forming a subgrain boundary (dashed line). This allows the relative rotation of the basal planes in the the undeformed regions, known as subgrains, eventually forming two individual grains separated by the angle* 2α.

break it in two, creating two new slightly differently orientated grains. This process is known as rotation recrystallization or polygonization. The event is shown in Figure 2.7. Dislocations organize between undeformed regions termed *subgrains*, forming a *subgrain boundary* [Alley, 1992]. The presence of dislocations thus facilitates the process, so primarily strained crystals are expected to recrystallize. Several studies assume that rotation recrystallization cannot occur until dislocation densities have reached a critical value at a certain depth, e.g. [Montagnat and Duval, 2000]. Below this point the fragmentation precisely outweighs the normal grain growth, explaining the stagnation in observed mean crystal size below $700\,m$ at GRIP. This explanation is probably not entirely correct as the formation of subgrains can be observed at all depths, in fact even in the firn (Sepp Kipfstuhl, personal communication).

An alternate explanation is offered by Mathiesen et al. (2004). NorthGRIP texture was examined, by analytically finding the solutions of a simple two-parameter

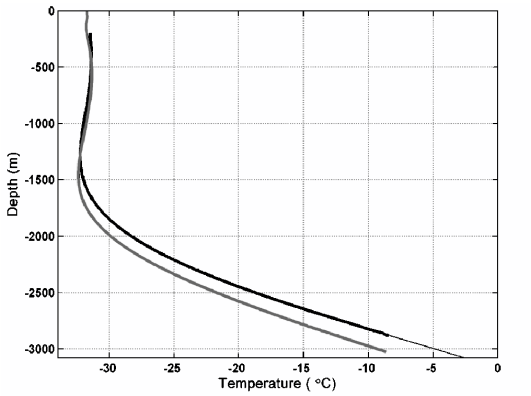

Figure 2.8: *The vertical temperature profiles at GRIP (grey line) and North-GRIP (black line). The temperatures are measured directly in the boreholes. The basal temperature at NorthGRIP is at the pressure melting point. Figure from Dahl-Jensen et al. (2003).*

differential equation, expressing the change in the grain size distribution by a diffusion term corresponding to the normal grain growth law along with a simple term for a fragmentation-rate proportional to grain diameter. In this model rotation recrystallization occurs throughout the core, but in the upper region (above $700\,m$) the effect of normal grain growth predominates. The parameters are tuned to match the evolution of mean grain size, but the modelled grain size *distributions* show remarkable agreement with observations, making the model very promising, though it has yet to be tested on other cores.

While rotation recrystallization could potentially influence fabric, it is poorly understood. Some authors speculate that it will slow down the evolution of fabric, e.g. [Thorsteinsson, 2002, Castelnau et al., 1996b], although, as will be discussed in Chapter 4, this may not be justified.

Migration Recrystallization

Near the base of the large ice sheets, temperatures are often near the pressure melting point due to the geothermal heat flux, see Figure 2.8. At these tem-

peratures strained grains can free the energy bound in dislocations by rapidly forming a new strain free grain, using remnants of old grains as seeds. The new grains are believed to have orientations favoring flow [Alley, 1992], i.e. such that the resolved shear stress on the basal plane is maximized. The decrease in fabric strength in the bottom part of GRIP and NorthGRIP is expected to be the result of migration recrystallization. However, not all authors agree about this. At the bottom simple shear usually dominates the deformation. It is often assumed that the simple shear deformation enhances the vertical fabric, whereas migration recrystallization acts to weaken the orientation, e.g. [Alley, 1992]. However modelling by van der Veen and Whillans using a formulation of Sachs' flow law (described in Section 3.3) suggested the opposite result. I shall briefly return to this problem in Chapter 4.

2.4.2 Effects of Impurities

The presence of soluble and insoluble impurities in the ice can affect the microstructure of ice. Particularly the insoluble impurities are expected to concentrate in the inter-grain boundaries, pinning them, and thus inhibiting the normal grain growth [Alley and Woods, 1996, Durand et al., 2006b]. This likely explains the sudden decrease in grain size observed across the Climatic Transition at Greenland ice cores, as Wisconsin dust concentration is high [Ruth et al., 2003]. The decrease in grain size, to half linear size across a depth interval of only $200\,m$, is unlikely to be explained by the low surface temperature in the Wisconsin, since the temperature difference between early Holocene and late Wisconsin ice is diminished by heat diffusion. Alternatively temperature dependant variations in the structure of precipitating snow could possibly lead to varying initial grain sizes at the firn-ice transition. It must, however, be stressed that this is unlikely to explain the small Wisconsin grains, as *memory* of initial sizes is likely to be extinguished during the rotation recrystallization regime.

It is plausible that the pinning of boundaries could effect the fabric, although no change in fabric is observed across the transition at GRIP. The degree of orientation at NorthGRIP is seen to evolve at a slightly reduced rate below the transition, but the interpretation is uncertain.

Chapter 3

Theory of Ice Flow

This Chapter presents various approaches to model the flow of ice. The theoretical background for the anisotropic flow models constructed in Chapter 4 will be provided. Furthermore the important empirically based Dansgaard-Johnsen model is described, as it will enable the comparison of the anisotropic models with the observations described in Chapter 2.

3.1 The Dansgaard-Johnsen Model

The Dansgaard-Johnsen model, known as the kink model, is a simple model for the flow of ice inside an ice sheet. In contrast to more advanced flow models relating the strain rates to the stress at each point in the ice sheet, the Dansgaard-Johnsen model is based entirely on mass balance along with a simple assumption for the vertical profile of the horizontal velocity.

The primary purpose of the model is to provide an age-depth relationship when other forms of dating, like stratigraphic layer counting, is unavailable. It therefore forms an important tool when prospecting new drill sites and for corrections of upstream effects.

3.1.1 Flow Line

It is instructive first to apply the Dansgaard-Johnsen model to a flow line, to illustrate the principle involved. Let the x-axis be the direction of horizontal flow e.g. perpendicular to an ice divide, and define the y-axis to be horizontal normal to the x-axis and z-axis to be vertical and positive upwards. Then define u, v, w to be the corresponding velocities. As this model is only concerned with the flow of *ice*, the effects of firn to ice transitions can be ignored by expressing accumulations and thickness in ice-equivalents.
The following assumptions are usually made for the flow line:

1. The direction of the horizontal component of flow is independent of depth and all components of strain orthogonal to this direction are zero.

2. The horizontal velocity, u, in the ice sheet is constant with depth from the surface to height h above the bedrock, and decreases linearly to the basal sliding velocity at the bottom, given by the fraction, FB, of the surface velocity.

3. Mass balance is assumed, meaning the thickness of the ice sheet, H, at every point is constant in time.

4. The net accumulation pr. area, a, is spatially constant, but temporal variations are allowed.

5. The basal melt rate pr. area, w_b, is constant in time and space.

Assumption 2 can be expressed as

$$u(z) = \begin{cases} u_{sur} & , z > h \\ u_{sur}\left(\frac{1-FB}{h}z + FB\right) & , z < h \end{cases} \tag{3.1}$$

Consider a bulk of ice stretching from $x = x_0$ to $x = x_0 + \delta x$ (See Figure 3.1). By assumption 3 it must be in mass balance, so the accumulation, $a\delta x$, must balance

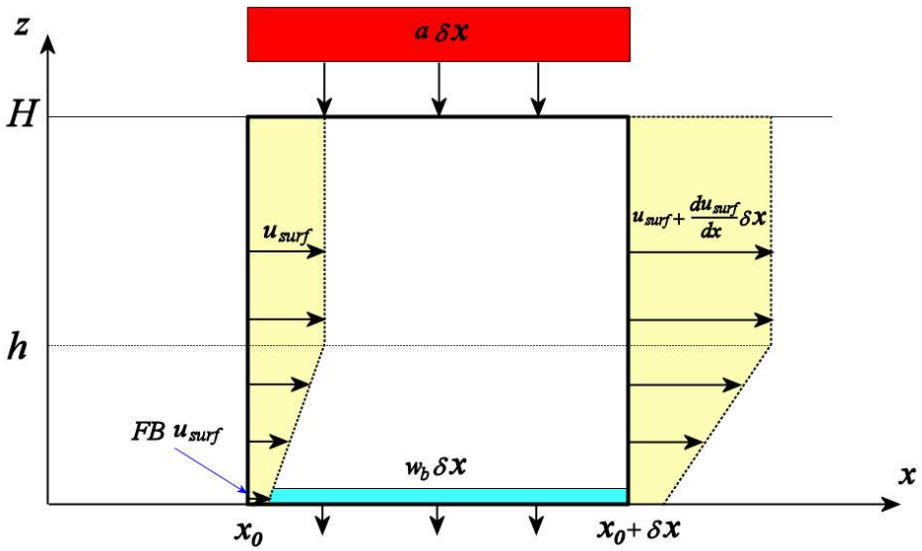

Figure 3.1: *Mass fluxes on a box of ice stretching from x_0 to $x_0 + \delta x$ along a flow line in the x-direction. The annual accumulation, $a\delta x$, is added to the volume; the basal melt, $w_b\delta x$ is removed, while the net outflow in the x-direction is $\delta x \int_0^H \frac{\partial u}{\partial x} dz$. For mass balance the total flux must be zero.*

the basal melt, -$w_b\delta x$ and the net outflow in the x-direction

$$\left((a - w_b) - \int_0^H \frac{\partial u}{\partial x} dz\right) \delta x = 0 \tag{3.2}$$

The integral in (3.2) can be found after insertion of (3.1).

$$\begin{aligned} \int_0^H \frac{\partial u}{\partial x} dz &= \int_0^h \frac{\partial u}{\partial x} dz + \int_h^H \frac{\partial u}{\partial x} dz \\ &= \frac{\partial u_{sur}}{\partial x} \left((H - h) + h \cdot FB + \frac{h(1 - FB)}{2}\right) \end{aligned} \tag{3.3}$$

Inserting (3.3) and solving (3.2) for $\partial u_{sur}/\partial x$ yields

$$\frac{\partial u_{sur}}{\partial x} = \frac{a - w_b}{H - \frac{h}{2}(1 - FB)} \tag{3.4}$$

The horizontal surface velocity thus increases linearly with distance along the flow line as vertical sections must remove snowfall of an increasing area. Since $\partial v/\partial y = 0$ by assumption 1, the incompressibility of ice can be expressed

$$\frac{\partial u}{\partial x} + \frac{\partial w}{\partial z} = 0 \tag{3.5}$$

So $\partial w/\partial z$ can be found by inserting (3.1) in (3.5).

$$\frac{\partial w}{\partial z} = -\frac{\partial u_{sur}}{\partial x} \cdot \begin{cases} 1 & , z > h \\ (\frac{1-FB}{h} z + FB) & , z < h \end{cases} \tag{3.6}$$

$$\frac{\partial u_{sur}}{\partial x} = \frac{a - w_b}{H - \frac{h}{2}(1 - FB)} \tag{3.7}$$

Now to find the vertical velocity profile, (3.6) is simply integrated .

$$\int_0^z \frac{\partial w}{\partial z} dz = -\frac{\partial u_{sur}}{\partial x} \int_0^z \left(\frac{1 - FB}{h} z + FB \right) dz \qquad , z < h \tag{3.8}$$

$$\int_0^z \frac{\partial w}{\partial z} dz = -\frac{\partial u_{sur}}{\partial x} \left(\int_0^h \left(\frac{1 - FB}{h} z + FB \right) dz + \int_h^z dz \right) \qquad , z > h \tag{3.9}$$

Both sides of the equations (3.8-3.9) can be calculated directly. Using the limit: $w(0) = w_b$ it is found that

$$w(z) - w_b = - \begin{cases} \frac{\partial u_{sur}}{\partial x} (\frac{(1-FB)z^2}{2h}(1 - FB) - FB \cdot z) & , z < h \\ \frac{\partial u_{sur}}{\partial x} (z - \frac{h}{2}(1 - FB)) & , z > h \end{cases} \tag{3.10}$$

In the upper layers of the ice sheet ($z > h$), the vertical velocity decreases linearly with depth. The vertical velocity profile is very important, because it can be used to establish a depth-age relationship for the ice. Before exploring this further, the extension of this result to other flow patterns will be examined.

3.1.2 Dome and General Flow

At domes the vertical velocity profile is also (3.10) even though the flow pattern here changes the calculations above. Near an ideal dome the flow is cylindrically symmetric and ice streams radially away from the summit. Clearly this flow pattern requires ice parcels to be strained both along and orthogonal to their direction of flow effectively reducing the radial strain required to facilitate the mass transport. The vertical strain rate on the contrary, being tied to the kink profile, can be specified solely by the local net accumulation (minus basal melt)

because the local height of the ice sheet must be conserved and thus remains unchanged.

For an ideal dome this can easily be verified explicitly, using cylindrical coordinates (r, θ, z) with $r = 0$ at the dome. The mass balance equation (3.2) is replaced by

$$(a - w_b)\pi r^2 = 2\pi r \int_0^H u_r dz \tag{3.11}$$

equal to

$$(a - w_b) = 2 \int_0^H \frac{\partial u_r}{\partial r} dz \tag{3.12}$$

where u_r is the radial velocity. After rewriting the continuity equation in cylindrical coordinates, using the symmetry, as

$$\frac{\partial w}{\partial z} + \frac{\partial u_r}{\partial r} + \frac{u_r}{r} = 0 \tag{3.13}$$

and applying (3.3), it is seen that vertical strain rate is unchanged whereas the surface velocity is half that of the flow line scenario. In reality only the vertical strain rate is of interest, so the results from the flow line can be transferred to the dome.

As long as the horizontal velocity maintains the *kink* profile, so must the vertical strain rate. This in turn uniquely describes the vertical strain rate in terms of local net accumulation completely independent of the directions of the horizontal strain.

Similarly the requirement that accumulation is constant in space can be removed. Note that although this will not affect the local vertical strain rate it will change the time-depth relationships, as ice is advected horizontally from areas with different accumulations.

3.1.3 Thinning of Annual Layers

Let us now look more closely at the consequences of the Dansgaard-Johnsen model. In ice sheets, annual layers formed on the surface will sink towards the bottom gradually thinning by the horizontal stretching as new layers are formed atop. It is customary to denote the present-day thickness of each annual layer by λ. The ratio of the present layer thickness to the original thickness at the time of deposition, λ_0, gives the *thinning* or *accumulated vertical strain* at the depth of the layer.

Constant Accumulation

Assuming the accumulation and the basal melt rate is constant in time, then each annual layer must annually be vertically displaced by its own thickness by the steady-state assumption, that is

$$\lambda(z) = w(z) \quad , \quad a = const \tag{3.14}$$

If the accumulation is suddenly changed, then the vertical velocity must also change in accordance with (3.10) while the layer thickness does not change instantly, clearly breaking (3.14).

Varying Accumulation

Leaving the assumption of steady-state, it is still assumed in the following that all the model parameters, in particular h and H, are constant in time. If accumulation vary things complicate a bit; however, in the special case with no basal melting, the vertical velocity can be written

$$w(z,t) = a(t) \cdot W(z) \tag{3.15}$$

where W is a function depending only on z. In the time step, dt, any annual layer, λ, is reduced in thickness by

$$d\lambda = \lambda \frac{\partial w}{\partial z} dt = \lambda a(t) \frac{dW}{dz} dt = \frac{\lambda}{W} dW \tag{3.16}$$

using the definition of velocity. (3.16) does not take horizontal advection of annual layers into account; hence it is only valid where upstream effects can be ignored, e.g. at domes. Integrating (3.16) following an annual layer from the surface to height z then yields

$$\frac{\lambda}{\lambda_0} = W(z) \tag{3.17}$$

This important result show that when no basal melt is present thinning is independent of varying snowfall. In reality, temporal constancy of h and H is of course not strictly obeyed. In central Greenland, variations in ice thickness during the last 100 ky is less than 10%, which indicates that (3.17) is a reasonable approximation. At GRIP for instance, no basal melting occurs, allowing the use of the thinning as a depth scale, which will be exploited when predictions of the anisotropic models described in Chapter 4 are compared to observations.

When both accumulation varies and basal melt is present, the thinning is a function of the accumulation *history* and melt rate. Assuming knowledge of the model parameters $H, h, a(t), w_b, FB$ the thinning can still be found by numerically integrating the first equality of (3.16) for each particle path through space and time.

Time-Depth Relationships

The age of ice at height z_0 can then in principle be found by numerically integrating

$$dz = w(z,t)dt \tag{3.18}$$

backwards in time. However the model parameters must be determined in the process. Provided an ice core has been drilled at the site, the problem is in principle attacked as follows. The thickness of the ice H can be inferred from radiometry or measured directly from the core. For simplicity the basal melt rate is usually assumed constant in time. Using a simple form for the accumulation,

e.g. constant value in the Holocene, the remaining parameters can be estimated such that the model matches the Holocene dating from stratigraphy and reference events[1].

The original thickness of a layer is somewhat correlated to the $\delta^{18}O$ content of the layer as the accumulation is related to the surface temperature [Johnsen et al., 1995]. The original thickness of each $55\,cm^2$ of the ice column can thus be estimated. The position of all layers are then integrated back in time using (3.18) until the first $55\,cm$ is lifted entirely off the ice sheet. Iterating this procedure the ice can be dated and the accumulations can be put on a time scale. Note this is a bit simplified as the accumulation-$\delta^{18}O$ relation must be tuned as well.

3.2 Isotropic Flow Models

3.2.1 Tensor Notation

In order to describe the mechanical properties of ice a firm notation is required. To this end I will use matrix and tensor notation as suitable throughout most of the following chapters as it allows for a compact notation. The reader will be expected to have some prior knowledge on tensor math; however, a brief summary of central continuum mechanical concepts will be provided in this section. Einstein summation is assumed implicitly in the following.

[1] Volcanos or climatic events

[2] Any resolution can be chosen, and the value of $55\,cm$ has historic reasons only, since it corresponds to the length of the bags in which the ice cores are stored.

Stress

In continuum mechanics the local stress inside a material, $\mathbf{p_n}$, on a surface with normal vector $\mathbf{n}$ is defined as

$$p_{(\mathbf{n})i} \equiv \lim_{\delta A \to 0} \frac{\delta F_{(\mathbf{n})i}}{\delta A} \qquad , \quad i = (1,2,3) \tag{3.19}$$

where δA is the area of the surface and $\delta \mathbf{F}_{(\mathbf{n})}$ is the force exerted *on* the surface by the surrounding material. The part of the stress acting normal to the surface is termed *pressure* and the remaining part is termed *shear stress*. As a consequence of *Cauchy's stress hypothesis* there exist a tensor, the stress tensor $\boldsymbol{\sigma}$, such that the stress on any surface can be written

$$p_{(\mathbf{n})i} = \sigma_{ij}\, n_j \qquad , \quad i,j = (1,2,3) \tag{3.20}$$

The nine components of the stress tensor $\{\sigma_{ij}\}$ are independent of the direction of the normal, and depend only on position and time. The stress tensor can always be assumed symmetric, since otherwise finite torques would act on infinitely small volume elements.

When describing incompressible materials equal normal pressure applied to every side of a small cube can often be ignored (depending on the constitutive relation). Under these circumstances the *stress deviator*, $\boldsymbol{\sigma'}$, is usually employed

$$\sigma'_{ij} = \sigma_{ij} - \frac{1}{3}\delta_{ij}\sigma_{kk} \qquad , \quad i,j,k = (1,2,3) \tag{3.21}$$

where δ_{ij} is Kronecker's delta, thereby excluding the hydrostatic pressure.

In glaciers flow is very slow, so accelerating terms can be ignored. This imposes further bounds on the stress tensor since local stress equilibrium must be maintained everywhere. This can be expressed in the following 3 equations, known as the local stress equilibrium relation

$$\nabla_j\, \sigma_{ij} + g_i = 0 \qquad , \quad i,j = (1,2,3) \tag{3.22}$$

where $\mathbf{g}$ is gravity.

Strain

The movement and deformation of a body can be characterized by a vector field $\mathbf{u}(\mathbf{x}_0, t)$ which indicates the displacement of a particle with original position x_0. At time t, the new positions are

$$\mathbf{x}(\mathbf{x}_0, t) = \mathbf{u}(\mathbf{x}_0, t) + \mathbf{x}_0 \tag{3.23}$$

The displacement field also contains information about translation and rigid rotation of the body, which are generally related to the boundary conditions, not the internal stress state of the body. To establish a *flow law* for a material, a measure of the relative movements of neighboring points is required. If only small displacements are considered, the relative displacement near a point x_0 can be characterized by a linearization of the displacement field, namely by its Jacobian tensor

$$J_{ij}(\mathbf{x}_0, t) = \left.\frac{\partial u_i(\mathbf{x}, t)}{\partial x_j}\right|_{\mathbf{x}=\mathbf{x}_0} \tag{3.24}$$

$\mathbf{J}$ is sometimes called the *displacement gradient tensor*. The displacement of the point $\mathbf{x}_0 + d\mathbf{x}$, near $\mathbf{x}_0$, can then be written

$$\mathbf{x}(\mathbf{x}_0 + d\mathbf{x}, t) = \mathbf{x}_0 + \mathbf{J}(\mathbf{x}_0, t)d\mathbf{x} \tag{3.25}$$

(3.25) predicts the stretching and rotation of any material line passing x_0 in a small neighborhood. Like any tensor the Jacobian can be written as a sum of a symmetric tensor, $\boldsymbol{\epsilon}$, and an antisymmetric one, $\boldsymbol{\Omega}$ containing the rigid body rotation. $\boldsymbol{\epsilon}$, known as the strain tensor, is thus

$$\epsilon_{ij}(\mathbf{x}_0, t) = \frac{1}{2}(J_{ij} + J_{ji}) = \frac{1}{2}\left(\frac{\partial u_i(\mathbf{x}, t)}{\partial x_j} + \frac{\partial u_j(\mathbf{x}, t)}{\partial x_i}\right)\Bigg|_{\mathbf{x}=\mathbf{x}_0} \tag{3.26}$$

and contains all information on relative movement of material lines near the point $\mathbf{x}_0$

In the following notation, a dot above a tensor represent the rate of change

with respect to time, for instance

$$\dot{\epsilon}_{ij}(\mathbf{x}_0, t_0) \equiv \left.\frac{\partial \epsilon_{ij}(\mathbf{x}_0, t)}{\partial t}\right|_{t=t_0} \tag{3.27}$$

denotes the strain *rate*, whereas $\dot{\mathbf{J}}$ denotes the *velocity gradient tensor*. To keep things complicated the time derivate of $\boldsymbol{\Omega}$ is usually denoted $\boldsymbol{\omega}$, which will also be done here for consistency with other works. Furthermore, the explicit notation of time and space dependance is omitted.

The incompressibility of a material can be expressed, in terms of the strain rate tensor, as

$$\dot{\epsilon}_{ii} = 0 \qquad , \quad i = (1, 2, 3) \tag{3.28}$$

3.2.2 Glen's Law

The most commonly used isotropic flow law for ice is known as Glen's law. By prolonged testing of blocks of polycrystalline ice under compressive stresses between 1 and 10 bars at different temperatures, Glen established the following empirical relation between the vertical strain rate and stress (1955)

$$\dot{\epsilon}_{33} = \left(\frac{\sigma_{33}}{A}\right)^n \tag{3.29}$$

A is a constant depending on the temperature, and Glen found the value of n to be 3.2. If n was equal to one ice would show viscous Newtonian behavior. On the other hand in the limit $n \to \infty$ ice would behave like a perfectly plastic material of yield strength A. The intermediate behavior of ice between these extremes is called visco-plastic.

The flow law was later generalized by Nye (1957). Nye assumed that

1. Strain rate is unaffected by hydrostatic pressure. ϵ_{ij} therefore depends only on the stress deviator, σ'_{ij}, and temperature.

2. Ice is isotropic and the ratios of the strain rate components are proportional to the ratio of the corresponding components of the stress deviator.

These are classical assumptions also made in the theory of plasticity.

Assumption 2 can be expressed as

$$\dot{\epsilon}_{ij} = \lambda \sigma'_{ij} \tag{3.30}$$

where λ is a scalar, depending on temperature, to be determined. It should be noted that this is not the most general assumption that can be made for an isotropic material.

Tradionally the terms *effective strain rate*, $\dot{\epsilon}$, and *effective shear stress*, τ, are used instead of the second tensor invariants of $\dot{\boldsymbol{\epsilon}}$ and $\boldsymbol{\sigma'}$

$$2\dot{\epsilon}^2 = \dot{\epsilon}_{ij}\dot{\epsilon}_{ij} \tag{3.31}$$

$$2\tau^2 = \sigma'_{ij}\sigma'_{ij} \tag{3.32}$$

Now inserting (3.30) in (3.31) and applying (3.32) we obtain

$$2\dot{\epsilon}^2 = 2\lambda^2\tau^2$$

$$\text{so} \qquad \dot{\epsilon} = \lambda\tau \tag{3.33}$$

(3.33) relates the second tensor invariants of $\dot{\boldsymbol{\epsilon}}$ and $\boldsymbol{\sigma'}$. Again a more general flow theory would require the inclusion of the third invariants as well (remember that the first invariants are both zero).

To determine the value of λ the special case of Glen's experiment is used. Inserting (3.29) in (3.33) after considering the incompressibility of ice and the definition of the stress deviator, one obtains

$$\lambda = \frac{\tau^{n-1}}{A^n}$$

and inserting in (3.30) finally

$$\dot{\epsilon}_{ij} = \frac{\tau^{n-1}}{A^n}\sigma'_{ij} \tag{3.34}$$

(3.34) is the usual formulation of Glen's flow law. In contrast to the mass-balance models, the time evolution of ice sheets can be modelled by numerical integration of Glen's law along with the stress equilibrium equation (3.22), the equation of continuity (3.28), a temperature model and suitable boundary conditions for stress, mass-fluxes and temperature, see for example Dahl-Jensen (1989). Although ice in the upper part of an ice sheet is fairly isotropic, strong anisotropy exists in the lower parts, e.g. at the bottom of Dye3 an enhancement of horizontal shear by a factor of 3 over the isotropic prediction has been observed from borehole logging [Dahl-Jensen and Gundestrup, 1987]. A further study attributed this deviation at least in part to the effects of anisotropy [Thorsteinsson et al., 1999]. It is thus problematic to model real ice sheets with Glen's law. Sometimes it is attempted to reduce the error by introducing the enhancement factor, E_{ij}, which is the the ratio of the measured (actual) strain rate to the one predicted by Glen's law. However, this only moves the problem to determining the enhancement factor, which requires knowledge of the *actual* strains.

3.3 Anisotropic Flow Models

Some simple generalizations of the constitutive relation to transversely isotropic materials exists, e.g. to ice. Such a continuum description was developed by Johnson (1977), relating strain rate to the stress deviator through a simple tensor relation including three material parameters, reflecting the macroscopic flow properties, and an orientation tensor for the direction of anisotropy. While the Johnson model is an improvement to Glen's law, it is also limited in its inability to predict the flow induced evolution of anisotropy, i.e. the fabric.

Since the ultimate goal of this work is to model the fabric evolution, the attention will focus on another type of models, which describe flow on individual grain scale. In these models, the macroscopic deformation of an aggregate of ice in response to an applied external stress deviator is determined from the deformation of individual grains. The stress and strain rate is assumed to be spatially constant inside each grain. This basically poses two problems, common to all these models

1. Given the applied external stress, $\boldsymbol{\sigma}$, the internal stress distribution of the aggregate must be determined, specifically by determining the stress acting on each grain, $\boldsymbol{\sigma}_{(g)}$.

2. The strain rate of an individual grain must be quantified in terms of the stress acting on it.

Traditionally two such models have been applied to ice, the Taylor-Bishop-Hill model [Bishop and Hill, 1951] (also known as the "upper bound" model) and the Sachs' model [Sachs, 1928]("lower bound"), representing two extreme ways of determining internal stresses.

The Taylor-Bishop-Hill model originates from metallurgy. This model assumes that the internal stress is configured such that the homogenous strain will occur in the aggregate. This removes any problems of overlapping grains or gaps emerging as a result of spatial variations in strain; however the stress equilibrium will be violated. To allow arbitrary deformation of a crystal, five independent slip systems is needed [Castelnau et al., 1996a]. When modelling ice this requires the activations of very *hard* slip systems, which is unrealistic, since individual crystals deform mainly by basal glide.

Sachs' model assumes that the stress on each crystal is equal to the macroscopic stress applied to the aggregate, and individual grains are only allowed to deform by basal glide. In this scenario the deformation of neighboring grains will be incompatible, since ice crystals best aligned for basal shear will deform the fastest. Intercrystal accommodation could possibly still be achieved by grain boundary processes such as surface diffusion and boundary sliding. However, because the *soft* crystals deform the fastest loads will eventually concentrate on crystals poorly aligned for flow, thus breaking the homogenous stress assumption.

A newer model introduced by Azuma (1994) will be investigated thoroughly. It is similar to Sachs' model, in the sense that individual grains are only allowed to deform by basal glide. Unlike Sachs' model, the internal stress distribution of the ice aggregate is determined by an empirically based relation in Azuma's model, as examined in Section 3.3.2. In this distribution, stress concentrates on hard grains, but to a lesser extent than in the Taylor-Bishop-Hill model.

For consistency, Azuma's and Sachs' model will apply identical quantifications of the strain rate-stress relations on individual grains in this presentation (Section 3.3.1), though it should be noted that this implies a slight but unimportant modification to the original formulation of Sachs' model.

3.3.1 Deformation of Individual Crystals

The first step is to relate the stress acting on an individual crystal to the deformation of the crystal. The deformation of an ice crystal can be compared to that of a deck of cards, easily deformed by shear in the basal plane but very hard to deform otherwise. When modelling ice, it is usual only to allow deformation of crystals by shear in the basal plane, because other slip systems are about 100 times harder to activate [Duval et al., 1983]. As the deformation of each grain

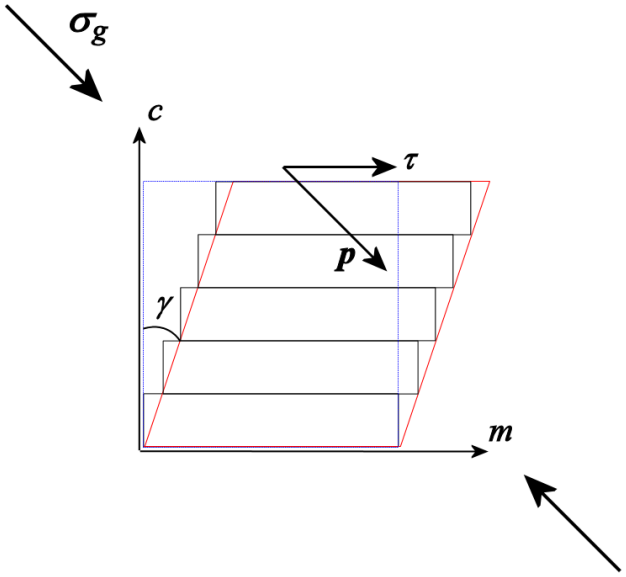

Figure 3.2: *Grain exposed to the stress $\boldsymbol{\sigma}_g$ leading to a force* **p** *on the basal plane. As ice only deforms by basal glide only the length of the projection of* **p** *on the basal plane, τ, and its direction,* **m**, *affects the deformation. The result is a shear displacement of γ.*

is assumed uniform, any crystal deformation can be described by one unit vector, the Burger vector **m** giving the direction of the shear[3] and the scalar, basal angular displacement, γ, see Figure 3.2.

Resolved Shear Stress

Now consider a grain, (g), with orientation $\mathbf{c}_{(g)}$ exposed to the stress[4] $\boldsymbol{\sigma}_{(g)}$ and denote the crystal basal plane $\mathbb{B}_{(g)}$. The stress acting on the basal plane of the crystal will then be

$$\mathbf{p}_{(g)} = \boldsymbol{\sigma}_{(g)}\mathbf{c}_{(g)} \tag{3.35}$$

[3]The Burger vector is denoted differently here than in Chapter 2, since in this model formulation it can have any direction in the basal plane, whereas the *true* microscopic Burger vector can only attain three distinct directions.

[4]The stress and its deviatoric part can be used interchangeably in this model

Generally $\mathbf{p}_{(g)}$ will not be confined to the crystal plane; however as the crystal can only deform by shear any force acting perpendicular to the basal plane can be ignored. Thus only the projection of $\mathbf{p}_{(g)}$ onto the basal plane is used to find the deformation. For this calculation let

$$\mathbf{m}^{\perp}_{(g)} \equiv \frac{\mathbf{c}_{(g)} \times \mathbf{p}_{(g)}}{\left|\mathbf{c}_{(g)} \times \mathbf{p}_{(g)}\right|} \tag{3.36}$$

$$\mathbf{m}'_{(g)} \equiv \frac{\mathbf{c}_{(g)} \times \mathbf{p}_{(g)} \times \mathbf{c}_{(g)}}{\left|\mathbf{c}_{(g)} \times \mathbf{p}_{(g)} \times \mathbf{c}_{(g)}\right|} \tag{3.37}$$

Clearly $\left\{\mathbf{m}^{\perp}_{(g)}, \mathbf{m}'_{(g)}\right\}$ will be an orthonormal basis for $\mathbb{B}_{(g)}$, so the calculation of the projection of $\mathbf{p}_{(g)}$ onto $\mathbb{B}_{(g)}$ is straightforward

$$\begin{aligned} \mathrm{proj}_{\mathbb{B}_{(g)}}(\mathbf{p}_{(g)}) &= (\mathbf{p}_{(g)} \cdot \mathbf{m}^{\perp}_{(g)})\mathbf{m}^{\perp}_{(g)} + (\mathbf{p}_{(g)} \cdot \mathbf{m}'_{(g)})\mathbf{m}'_{(g)} \\ &= (\mathbf{p}_{(g)} \cdot \mathbf{m}'_{(g)})\mathbf{m}'_{(g)} \end{aligned} \tag{3.38}$$

(3.38) shows that the shear stress in the basal plane has magnitude (resolved shear stress)

$$\tau_{(g)} \equiv \left|\mathrm{proj}_{\mathbb{B}_{(g)}}(\mathbf{p}_{(g)})\right| = \mathbf{p}_{(g)} \cdot \mathbf{m}'_{(g)} \tag{3.39}$$

and direction $\mathbf{m}'_{(g)}$. In this formulation it is postulated that this is also the direction of slip. That is

$$\mathbf{m}_{(g)} = \mathbf{m}'_{(g)} \equiv \frac{\mathbf{c}_{(g)} \times \mathbf{p}_{(g)} \times \mathbf{c}_{(g)}}{\left|\mathbf{c}_{(g)} \times \mathbf{p}_{(g)} \times \mathbf{c}_{(g)}\right|} \tag{3.40}$$

This is a reasonable assumption, but not completely true, since the basal slip systems cannot achieve entirely arbitrary deformations[5]. Experimental investigation of single crystal ice, however, reveals no preferred direction of glide in the basal plane [Kamb, 1961].

[5]Note that this assumption is traditionally not made in Sachs' model. Instead the resolved shear stress is determined along three slip systems in the basal plane having fixed directions as determined by the microscopic Burger vector, **b**. This change is made only to clearly illustrate the important similarities and differences between Sachs' and Azuma's models, and does not change the predictions of the model.

The Schmidt Tensor

Before attacking the problem of finding a relationship between $\tau_{(g)}$ and $\gamma_{(g)}$ the Schmidt tensor, $\mathbf{S}_{(g)}$, is introduced to allow a shorter notation.

The Schmidt tensor for a crystal is defined as the outer product of the Burger vector and the c-axis of the crystal

$$\mathbf{S}_{(g)} \equiv \mathbf{m}_{(g)} \otimes \mathbf{c}_{(g)} \qquad \text{or equivalently} \qquad S_{ij(g)} \equiv m_{i(g)} c_{j(g)} \tag{3.41}$$

Utilizing the tensor form (3.35) and (3.41) allows (3.39) to be rewritten as

$$\tau_{(g)} = \mathbf{S}_{(g)} : \boldsymbol{\sigma}_{(g)} \tag{3.42}$$

This is just a handy change of notation. The Schmidt tensor will also prove to be useful in the coming sections.

Shear Displacement Rate of Basal Plane

When the resolved shear stress on a crystal $\tau_{(g)}$ is known, the angular displacement rate of H_2O planes, $\dot{\gamma}_{(g)}$ also known as the shear displacement rate of the crystal, can be determined by the empirical relation [Weertan, 1983]

$$\dot{\gamma}_{(g)} = \beta \tau_{(g)}^{n} \tag{3.43}$$

where β is the flow constant, which depends on temperature. The value of the exponent n is somewhat situational but is usually taken to be three. Notice the close resemblance between (3.43) and (3.29). Unlike isotropic ice, deformation of single ice crystals are only allowed by shearing along their basal plane, but individual crystals do show a visco-plastic response to a given resolved shear stress on the basal plane.

The 'Laboratory' Frame of Reference

The strain of individual crystals in terms of angular displacement of individual crystal planes has been found. In order to make sense of this information, a

description of the deformations in the macroscopic frame of reference is needed. Let (x, y, z) denote the macroscopic fixed frame and let $(x'_{(g)}, y'_{(g)}, z'_{(g)})$ with axial unit vectors $(\mathbf{m}_{(g)}, \mathbf{m}^{\perp}_{(g)}, \mathbf{c}_{(g)})$ denote the microscopic frame of the crystal (g). The tensor of transformation from the microscopic to the macroscopic frame is readily found as

$$T = \begin{bmatrix} m_{1(g)} & m^{\perp}_{1(g)} & c_{1(g)} \\ m_{2(g)} & m^{\perp}_{2(g)} & c_{2(g)} \\ m_{3(g)} & m^{\perp}_{3(g)} & c_{3(g)} \end{bmatrix} \tag{3.44}$$

The shear displacement rate of the crystal can in the microscopic reference system can be described by the strain tensor.

$$\dot{\epsilon}'_{(g)} = \frac{\dot{\gamma}_{(g)}}{2} \begin{bmatrix} 0 & 0 & 1 \\ 0 & 0 & 0 \\ 1 & 0 & 0 \end{bmatrix} \tag{3.45}$$

The strain of crystal (g) as seen from the laboratory can now be calculated simply by transforming (3.45). With the use of (3.44) we obtain

$$\begin{aligned} \dot{\boldsymbol{\epsilon}}_{(g)} &= \mathbf{T}_{(g)} \dot{\boldsymbol{\epsilon}}'_{(g)} \mathbf{T}^{T}_{(g)} \\ &= \frac{\dot{\gamma}_{(g)}}{2} \left[m_{i(g)} c_{j(g)} + m_{j(g)} c_{i(g)} \right]_{ij} \\ &= \frac{\dot{\gamma}_{(g)}}{2} (\mathbf{S}_{(g)} + \mathbf{S}^{T}_{(g)}) \\ &= \dot{\gamma}_{(g)} \mathbf{S}^{(s)}_{(g)} \end{aligned} \tag{3.46}$$

where $\mathbf{S}^{(s)}_{(g)}$ is the symmetrical part of the Schmidt tensor. This concludes the description of a single ice crystal exposed to the stress $\boldsymbol{\sigma}_g$. As ice is an aggregate of many ice crystals the procedure is then to calculate the deformation of the aggregate as the average of individual crystal deformations possibly weighted by size, if information is available. This however requires knowledge of $\boldsymbol{\sigma}_g$ for every crystal. As already discussed, in Sachs' model this is done simply by assuming that the stress on each crystal is equal to the applied macroscopic stress. The next section presents Azuma's improvements to this crude assumption.

3.3.2 Azuma's Model

The important problem of determining the stress distribution inside an ice aggregate cannot be observed directly. Empirical investigations in the laboratory must instead examine the stress indirectly by measuring the strain of individual crystals when an external load is applied to a sample. Unfortunately individual crystals in the ice can only be observed by thin sectioning of the sample, thereby destroying the sample and consequently removing the possibility of making consecutive measurements.

Instead Azuma and Higashi (1985) made a 2-dimensional study of ice flow, which was later refined [Azuma, 1995], to estimate internal stress configurations. In this study, ice was prepared in thin sections $2mm$ thick of area $20x30mm$. The samples were cut from artificial ice, consisting of columnar ice crystals with horizontal orientation grown on a water surface. The samples were then mounted between two glass plates, thereby fixing the thickness of the samples and preventing buckling during the deformation tests. The samples were cut such that c-axes were confined to the plane of the thin section, thereby allowing individual crystals to deform by basal glide with no components of the strain orthogonal to the thin section plane. The samples were then compressed uniaxially along their long axis. Tests have been carried out at different temperatures ranging from 253-263K and with loads of 0.1Mpa. As the sample deforms individual crystals are observed through crossed polaroids. Fabrics can be determined both before and during the deformation tests using the standard optical method [Langway, 1958]. The strain of individual crystals can be found by following the relative movement of air bubbles. Since deformation inside each crystal is not ideally uniform a least square fit was used. For different bulk strains Azuma thus obtained corresponding sets of orientation and vertical strain of individual ice crystals. The strain is taken as a measure of the strain rate since strain rate is assumed to be constant

in time for the small strains observed here.

Schmidt Factor

In tests of uniaxial compression, it is useful to introduce the Schmidt factor, S_g, for each grain

$$S_g = \cos\chi_g \sin\chi_g \tag{3.47}$$

where χ_g is the angle between the normal of the c-axis and the axis of compression. Let σ_g be the applied pressure and let $\dot{\epsilon}_g$ be the vertical strain rate of grain (g). It can then be shown that the Schmidt factor relates the resolved shear stress and the shear strain rate of the basal plane to the macroscopic axial stress and strain rate of the crystal by

$$\tau_g = S_g \sigma_g \tag{3.48}$$

$$\dot{\epsilon}_g = S_g \dot{\gamma}_g \tag{3.49}$$

Since the resolved shear stress on the basal plane is proportional to the Schmidt factor, it can be interpreted as a measure of how well a grain is aligned for basal glide. Also notice the close formal similarity between (3.48) and (3.49) in the uniaxial case and (3.42) and (3.46) in the general case. Inserting (3.48) and (3.49) into (3.43) the deformation of individual crystal can be expressed in the macroscopic system

$$\dot{\epsilon}_g = \beta \sigma_g^n S_g^{n+1} \tag{3.50}$$

Testing Distributions of Stress

Azuma (1995) tested the assumption of uniform stress, i.e. Sachs' model, on his data. If stress is uniform (3.50) reduces to

$$\dot{\epsilon}_g = \beta \sigma_{bulk}^n S_g^{n+1} \tag{3.51}$$

Figure 3.3a shows the Schmidt factor plotted vs. vertical strain of each grain. It was concluded that (3.51) disagreed with the data no matter the choice of n, thus

the hypothesis of uniform stress was rejected. Uniform strain was not observed either.

In his first study Azuma (1985) instead claimed data fits red dotted line shown in Figure 3.3a, such that

$$\epsilon_g = \pi \epsilon_{bulk} S_g \tag{3.52}$$

From (3.49) and (3.52) it is seen that $\gamma_g = \epsilon_g / S_g = \pi \epsilon_{bulk}$ meaning that stress will be distributed such that the shear strain and consequently the resolved shear stress on every crystal will be the same. However, the data does not clearly support (3.52), as data scatters a lot. This led Azuma to the idea that the strain of a crystal was not merely dependent on the orientation of the crystal itself, but also on that of adjacent crystals. Azuma introduced S_L and ϵ_L, the *local mean* of the Schmidt factor and vertical strain respectively. The local mean of a quantity surrounding a crystal is defined as its average value for the crystal itself and adjacent ones, i.e.

$$\epsilon_L = \frac{1}{N} \sum_{i=1}^{N} \epsilon_{(g)i} \tag{3.53}$$

$$S_L = \frac{1}{N} \sum_{i=1}^{N} S_{(g)i} \tag{3.54}$$

where i ranges over the grain and its $N-1$ neighbors. S_g/S_L vs. ϵ_g/ϵ_L is plotted in Figure 3.3b which clearly demonstrates that

$$\frac{\epsilon_g}{\epsilon_L} = \frac{S_g}{S_L} \tag{3.55}$$

(3.55) states that when the vertical strain ϵ_L is imposed on a small region of the aggregate, the deformation of each grain inside the region is scaled by $\frac{S_g}{S_L}$. This result and (3.52) are in fact very similar. Indeed, if the notion of local area was extended to encompass the entire bulk of ice, then (3.52) and (3.55) would be equivalent.

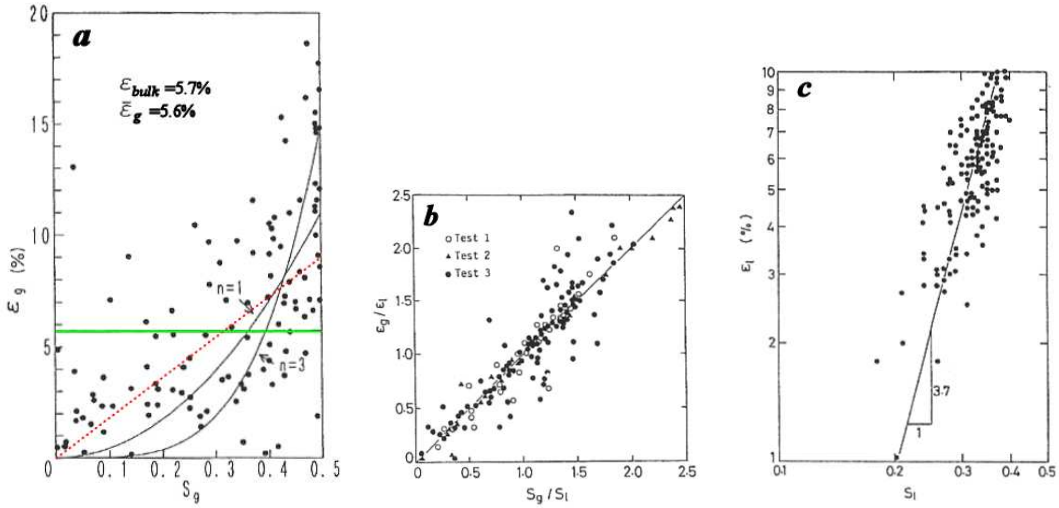

Figure 3.3: *Data from Azuma's compression experiment (1995). A thin section of ice was compressed, undergoing a vertical strain of* 5.7%. **a**. *The orientation of individual grains (Schmid factor) vs. the vertical strain on the grain (dots). The green line shows the theoretical prediction by the Taylor-Bishop-Hill model that all grains undergoes equal vertical strain. The black curves shows predictions of Sachs' model for the different values of the flow exponent, n, and the red dotted line corresponds to Azuma's first assertion that all grains undergoes equal basal shear displacement* (3.52). *The data scatters a lot, implying no functional relationship exists between S_g and ϵ_g.* **b**. *When plotting the Schmid factors and vertical strains for each grain relative to their respective local mean surrounding the grain, equality is observed leading to* (3.55). *The results from three test samples are shown marked by circles, triangles and dots.* **c**. *Plot shows a log-log plot of the local mean Schmidt factor surrounding each grain vs. the local mean vertical strain around the grain. The assumed stress distribution* (3.56) *implies the relation* (3.57), *which predicts a straight line of slope* $n + 1$.

Azuma (1995) then made the hypothesis that the distribution of stress is given by

$$\sigma_g = \frac{S_L}{S_g}\sigma_{bulk} \tag{3.56}$$

such that stress will concentrate on hard grains and more so if the grain is surrounded by softer grains. Following the argument of Azuma (3.55) and (3.56) is then inserted into (3.50) yielding

$$\dot{\epsilon}_L = \beta\sigma_{bulk}^n S_L^{n+1} \tag{3.57}$$

When log-log-plotting ϵ_L vs. S_L^{n+1} (3.57) predicts a straight line with slope $n+1$. After looking at his data (Figure 3.3c) Azuma accepted (3.56) and found a value of $n = 3$ to be reasonable.

The observant reader may wonder why Azuma, after finding the relationship between deformation and orientation (3.55) and accepting the relationship between stress and deformation (3.43), not merely derives (3.56) from these, instead of testing it against data. The short answer to that question is that (3.55) and (3.43) lead to a slightly different and more complicated distribution of stress, but (3.56) serves as a very good approximation in which the stress on a grain depends only on the orientations of the grain and immediately adjacent grains.

General Stress Situation

Having determined the internal distribution of the vertical component of stress for a uniaxial external load applied to the aggregate, the next step was to determine the internal stress distribution, $\boldsymbol{\sigma}_g$, for an arbitrary external stress, $\boldsymbol{\sigma}$ [Azuma, 1994]. In the following the external frame of reference is chosen such that $\boldsymbol{\sigma}$ has a diagonal representation, with diagonal elements $\sigma_1, \sigma_2, \sigma_3$ denoting the three principal stresses acting macroscopically on the aggregate. Azuma then

made the following assumption:
The stress acting on each grain, $\boldsymbol{\sigma}_g$, has the same principal axes as the macroscopic stress, $\boldsymbol{\sigma}$. The principal stress acting along each axis is distributed as given by (3.56) independently of the other directions, that is

$$\sigma_{(g)i} = \frac{S_{(L)i}}{S_{(g)i}}\sigma_i \qquad (i = 1, 2, 3) \tag{3.58}$$

where S_i denotes the Schmidt factor with respect to axis i. Using the definitions (3.41) and (3.47) it can be verified that S_1, S_2, S_3 are in fact the diagonal entries of the Schmidt tensor. Exploiting that a reference system with a diagonal stress tensor was chosen, the generalized microscopic distribution of stress (3.58) is inserted in (3.42)

$$\begin{aligned} \tau_{(g)} &= \mathbf{S}_{(g)} : \boldsymbol{\sigma}_{(g)} \\ &= S_{(g)ij}\sigma_{(g)ij} \\ &= S_{(g)i}\frac{S_{(L)i}}{S_{(g)i}}\sigma_i \\ &= \mathbf{S}_{(L)} : \boldsymbol{\sigma} \end{aligned} \tag{3.59}$$

(3.59) was derived in a special frame of reference only to clarify the assumptions and calculations, it is valid in any frame of reference. This concludes the search for the internal stress distribution of an aggregate of ice.

The constitutive relation

Given the stress acting on an ice aggregate, (3.59) predicts the resolved shear stress on individual grains, which in turn determines the strain of each grain with the use of (3.43) and (3.46). The evolution of individual grain sizes is not modelled, so the strain rate of the aggregate is assumed simply to be the arithmetic mean of the strain rates of the grains (3.60). Together these equations form

a constitutive relation for ice and are repeated here for the sake of completeness

$$\tau_{(g)} = \mathbf{S}_{(L)} : \boldsymbol{\sigma} \tag{3.59}$$

$$\dot{\gamma}_{(g)} = \beta \tau_{(g)}^{n} \tag{3.43}$$

$$\dot{\boldsymbol{\epsilon}}_{(g)} = \dot{\gamma}_{(g)} \mathbf{S}_{(g)}^{(s)} \tag{3.46}$$

$$\dot{\boldsymbol{\epsilon}} = \left\langle \dot{\boldsymbol{\epsilon}}_{(g)} \right\rangle \tag{3.60}$$

These relations require great computational efforts compared to the simplicity of Glen's law, as the strain of every single grain is calculated. Contrary to Glen's law the all important effects of anisotropy are accounted for, though the fabric must be specified. Unfortunately the fabric will change as ice flows, and the constitutive relations contain no information of the rotation of material lines, because only the symmetric part the displacement tensor is accounted for. Hence, it is often useful to couple Azuma's model to a fabric evolution model. This is the topic of the next section.

3.3.3 Rotation of Crystallographic Axes

It is a well established empirical fact that the orientation of a grain changes as it deforms. Both in situ measurements and laboratory experiments confirm that c-axes will migrate towards the axis of compression. It is important to realize that the c-axis of a grain is *not* a material line, so the rotation of the c-axis does not necessarily imply a rotation of the grain as such. Rather a grain deforming by basal glide must be rotating if its c-axis is not.

In this section two different theoretical quantifications of this rotation are derived, the Lister model and the Schmid-Boas model.

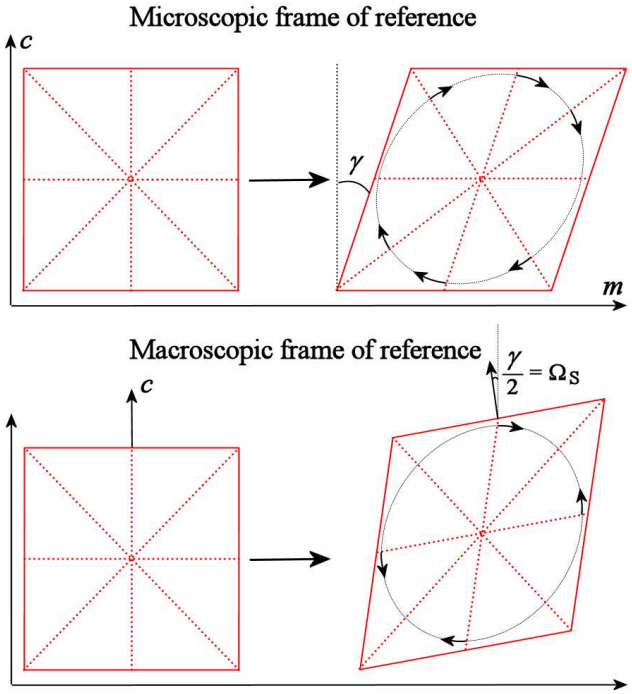

Figure 3.4: *A grain undergoing the shear deformation, γ, by glide in the basal plane.* **Top***: The microscopic frame. With respect to its own axes the grains deform by simple shear implying a (clockwise) rotation of the material lines (red dotted lines).* **Bottom***: According to the Lister model the material lines of grains must not rotate, when seen from the macroscopic frame, if the ice bulk is undergoing rotation free deformation. In this frame individual grains thus deform by pure shear, changing the orientation of the c-axis by $\Omega_C = \gamma/2$. If the bulk is undergoing rotation, it must be added to the rotation of the c-axis.*

Lister

Recall that individual ice crystals deform by simple shear *with respect to their internal axes* and that the velocity gradient tensor associated with simple shear can be resolved into a pure shear deformation and a rigid body rotation.

$$\dot{\mathbf{J}}' = \dot{\boldsymbol{\epsilon}}' + \boldsymbol{\omega}_S' = \frac{1}{2}\begin{bmatrix} 0 & 0 & \dot{\gamma}_g \\ 0 & 0 & 0 \\ \dot{\gamma}_g & 0 & 0 \end{bmatrix} + \frac{1}{2}\begin{bmatrix} 0 & 0 & \dot{\gamma}_g \\ 0 & 0 & 0 \\ -\dot{\gamma}_g & 0 & 0 \end{bmatrix} \tag{3.61}$$

As ice flows, (3.61) shows that the vorticity of each grain with respect to its internal axes is $(0, \dot{\gamma}_g/2, 0)$[6]. Rewriting (3.61) in the macroscopic frame of reference yields

$$\dot{\mathbf{J}} = \dot{\boldsymbol{\epsilon}} + \boldsymbol{\omega}_S + \boldsymbol{\omega}_C \tag{3.62}$$

where $\boldsymbol{\omega}_C$ is the rotation of the c-axis as seen from the macroscopic system, see Figure 3.4. Using (3.44), the rotation associated with the simple shear of the grain is transformed to the macroscopic frame by

$$\begin{aligned} \boldsymbol{\omega}_S &= \mathbf{T}_{(g)} \dot{\boldsymbol{\omega}}_S{}' \mathbf{T}_{(g)}^T \\ &= \frac{\dot{\gamma}_{(g)}}{2}\left[m_{i(g)}c_{j(g)} - m_{j(g)}c_{i(g)}\right]_{ij} \\ &= \frac{\dot{\gamma}_{(g)}}{2}(\mathbf{S}_{(g)} - \mathbf{S}_{(g)}^T) \\ &= \dot{\gamma}_{(g)}\mathbf{S}_{(g)}^{(a)} \end{aligned} \tag{3.63}$$

where $\mathbf{S}_{(g)}^{(a)}$ is the antisymmetric part of the Schmidt tensor, which comes in handy once again.

Modelling quartzite using the Taylor-Bishop-Hill model, Lister et al. (1978), proposed a model for the rotation of crystallographic axes. As the material deforms a specific deformation is imposed on every grain, in the case of the Taylor-Bishop-Hill model, the deformation of the aggregate. Specifically the *vorticity of any*

[6]The (relative) vorticity, $\bar{\boldsymbol{\omega}}$, is related to the antisymmetric rotation tensor by $\bar{\boldsymbol{\omega}} \equiv \nabla \times \dot{\mathbf{u}} = (\omega_{23}, \omega_{13}, \omega_{12})$

grain must be equal to the vorticity of the imposed deformation. It is not clear if this requirement can be directly transferred to ice deforming by basal glide, since only two independent slip systems are available. In this case, the imposed deformation on a grain is likely not equal to the deformation of the aggregate, since neighboring grains are also limited to two slip systems. Regardless of this violation of the assumptions to the Lister model, it is usual also to assume for ice (e.g. [Thorsteinsson, 2002, van der Veen and Whillans, 1994]) that
The vorticity of any grain with respect to the macroscopic axes is equal to the vorticity of the deformation of the aggregate.
Using (3.62), this can be expressed as

$$\boldsymbol{\omega}_b = \boldsymbol{\omega}_S + \boldsymbol{\omega}_C \tag{3.64}$$

where $\boldsymbol{\omega}_b$ is the rotation of the imposed deformation of the aggregate (termed bulk rotation), which must be specified by a boundary condition. The bulk rotation is zero for irrotational deformations of the aggregate, such as uniaxial tension/compression and pure shear, while a horizontal simple shear of the xz-plane implies the boundary condition $\omega_{(b)13} = \dot{\epsilon}_{13}$.

Since the ground work is already done, the necessary rotation of the c-axis as seen from the macroscopic frame can be found, rearranging (3.64) and inserting (3.63), to be

$$\boldsymbol{\omega}_C = \boldsymbol{\omega}_b - \dot{\gamma}_{(g)}\mathbf{S}^{(a)}_{(g)} \tag{3.65}$$

(3.65) must be determined for each grain. The new direction of the c-axis vector of grain (g) after the time step, dt, can then be found as

$$\mathbf{c}_{(g)}(t_0 + dt) = \mathbf{c}_{(g)}(t_0) + \boldsymbol{\omega}_C\mathbf{c}_{(g)}(t_0)dt \tag{3.66}$$

where t_0 is the initial time.

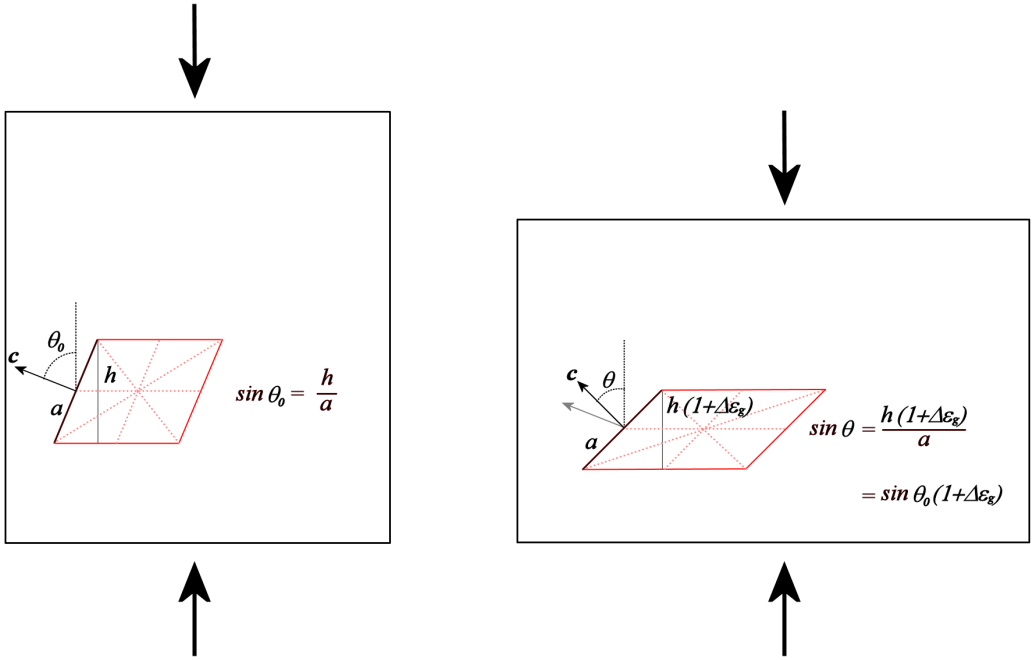

Figure 3.5: *The Schmid-Boas model. A bulk of ice undergoing uniaxial vertical compression. The vertical strain ϵ_g is imposed on an individual grain undergoing the deformation shown, by glide in the basal plane (plane normal to* **c***) and a rigid body rotation. There is no rotation of the horizontal material lines of the grain. Since the basal plane is undistorted by the deformation, the 'length' of the basal plane, a, is unchanged, allowing the derivation of* (3.67).

Schmidt and Boas

Schmid and Boas (1935) described a different model for the c-axis rotation of a grain undergoing a specified deformation. In this model it is postulated that crystals deforming by basal glide undergoing uniaxial compression are only allowed to deform as shown in Figure 3.5, due to constraints imposed by neighboring grains. When the vertical strain, $\epsilon_{(g)z}$, is imposed on a grain of initial orientation (polar angle) θ_0, the new orientation of the grain is given by

$$\sin\theta = (1 + \epsilon_{(g)z}) \sin\theta_0 \tag{3.67}$$

The assumption is that in each grain the material lines perpendicular to the axis of compression remain unrotated. In the case of uniaxial extension applied to the ice bulk, it is similarly postulated that there is no rotation of material lines parallel to the axis of extension leading to the relation

$$\cos\theta = (1 + \epsilon_{(g)z})^{-1} \cos\theta_0 \tag{3.68}$$

The basis for these assumptions is not given. The lattice rotation is thus dependent of the type of stress applied, and it is not clear how to extend these relations to a general stress state.

This model was originally constructed to determine the reorientation of individual grains directly from an imposed vertical bulk strain. In order to combine this model with Azuma's model, (3.67) and (3.68) need to be expressed as the rotation of the c-axis in terms of the shear displacement of the basal plane. As shown in Appendix B, (3.67) and (3.67) can be rewritten as

$$\boldsymbol{\omega}^C = -2\sin^2\theta\dot{\gamma}_{(g)}\mathbf{S}^{(a)}_{(g)} \qquad \text{vertical bulk compression} \tag{3.69}$$

$$\boldsymbol{\omega}^C = -2\cos^2\theta\dot{\gamma}_{(g)}\mathbf{S}^{(a)}_{(g)} \qquad \text{vertical bulk extension} \tag{3.70}$$

respectively. The c-axis vector of each grain can then be found using (3.66).

Chapter 4

Simulating Fabric Evolution

This chapter presents an implementation of the models described in the previous chapter. The evolution of fabric is examined using Azuma's model for anisotropic ice flow along with both Lister's and Schmid-Boas' model for grain rotation. First, the model is tested in the simplest stress configuration and compared to laboratory deformation tests.

4.1 The Model

My implementation of Azuma's model is coded in Matlab. Initial fabric for an ice aggregate of N crystals is designated. Specifying an external stress field, $\boldsymbol{\sigma}$, acting on the aggregate, the bulk strain and fabric evolution can be numerically integrated using an iterative scheme as follows:

1. The strain rate of each grain with respect to its own axes is calculated using (3.43) and (3.59).

2. A suitable time step is chosen, e.g. such that $\dot{\gamma}_g dt < 1\%$ for every grain.

3. The bulk strain during dt is calculated using (3.46) and (3.60).

4. The new fabric is either determined from the Lister rotation model (3.65) or the Schmid-Boas model (3.69) or (3.70).

5. Various recrystallization models can be inserted here.

6. The stress field and flow parameter, $A(T)$, is updated if necessary and the iteration is repeated.

Application of (3.59) requires definition of the *local area* surrounding a crystal $i \in \{1, 2, ..., N\}$. Taking a simple approach I define the *local area* of crystal i as

$$L_i = \{i - \eta, ..., i, ..., i + \eta\} \tag{4.1}$$

where 2η denotes the number of neighbors to any crystal influencing its softness. If $\eta = 0$ the flow law reduces to Sachs' model, while increasing values will make the resolved shear stress on the basal planes progressively more homogenous throughout the aggregate. I use a value of $\eta = 3$ when applying Azuma's model, giving each grain 6 neighbors, somewhat corresponding to grains arranged in a cubic grid.

4.2 Simulating Ideal Stress Configurations

Before turning the attention to the modelling of real ice fabrics, this model setup is tested in the simplest stress states for comparison with the original publication [Azuma, 1994].

4.2.1 Irrotational Deformation

Figure 4.1(*b-d*) shows examples of the modelled fabric resulting from three stress states: uniaxial vertical compression, uniaxial vertical extension and pure shear,

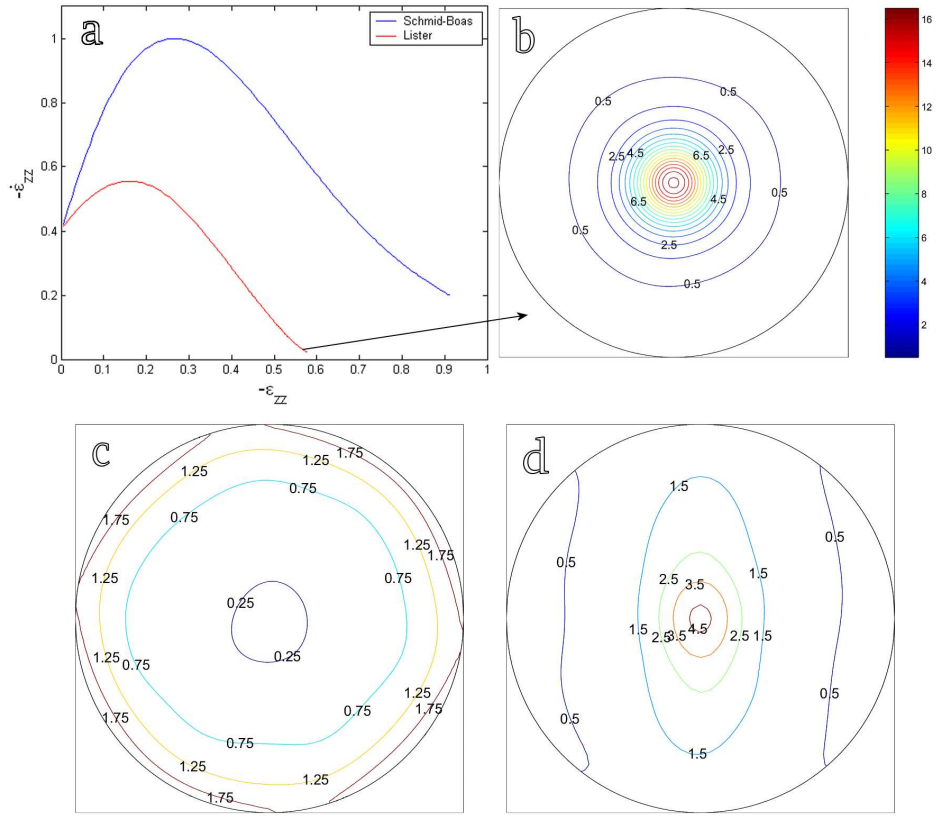

Figure 4.1: a. *The creep curve of polycrystalline ice for uniaxial compression for initial random orientation as predicted by Azuma's model in conjunction with Lister's and Schmid-Boas' rotation model.* **b-d**. *fabrics modelled by the Azuma/Lister model for uniaxial compression, uniaxial extension and pure shear respectively. These results are in agreement with Azuma (1994).*

respectively represented by the following Cauchy stress deviator tensors

$$\boldsymbol{\sigma}'_{uc} = \sigma' \begin{bmatrix} \frac{1}{2} & 0 & 0 \\ 0 & \frac{1}{2} & 0 \\ 0 & 0 & -1 \end{bmatrix} \qquad \boldsymbol{\sigma}'_{ue} = \sigma' \begin{bmatrix} -\frac{1}{2} & 0 & 0 \\ 0 & -\frac{1}{2} & 0 \\ 0 & 0 & 1 \end{bmatrix} \qquad \boldsymbol{\sigma}'_{ps} = \sigma' \begin{bmatrix} 1 & 0 & 0 \\ 0 & 0 & 0 \\ 0 & 0 & -1 \end{bmatrix}$$

These fabrics are modelled using Lister's rotation model, with the boundary condition for bulk rotation

$$\boldsymbol{\omega}_b = \mathbf{0} \tag{4.2}$$

In vertical compression the c-axes migrate towards the vertical axis and for vertical extension away from it towards the horizontal plane. Indeed, c-axes will always move towards compressive and away from the extensive axes, in the models presented here. This principle is exemplified by the formation of a girdle fabric under pure shear, which have one axis of extension and one axis of compression. These results are in agreement with Azuma (1994).

The evolution of fabric, in turn, affects the flow properties of the aggregate. Figure 4.1(a) shows the change in vertical strain rate of the aggregate as a function of vertical straining under constant uniaxial vertical compression. The aggregate is seen to *soften* with respect to vertical compression as it strains until it reaches a critical strain after which the strain rate decreases towards zero. This can be understood since the softest grains are aligned 45° to vertical, while grains in randomly oriented ice form the average angle of 60° to vertical. As the aggregate is compressed the average softness thus initially increases as favored orientation develops. Eventually the emerging vertical orientation will make the straining progressively difficult; this is known as strain hardening. Further vertical straining can then only be accommodated by the formation of new grains, aligned for flow, e.g. by migration recrystallization. Ice with nearly vertical fabric is instead aligned perfectly for simple shear deformation.

4.2.2 Rotational Deformations

Simple shear in the xz-direction of an aggregate is associated with the stress deviator

$$\boldsymbol{\sigma}'_{ss} = \begin{bmatrix} 0 & 0 & 1 \\ 0 & 0 & 0 \\ 1 & 0 & 0 \end{bmatrix} \tag{4.3}$$

which represents a pure shear with compression axis $(-1, 0, 1)/\sqrt{2}$ and extension axis $(1, 0, 1)/\sqrt{2}$. No information of the bulk rotation implied by the simple shear is contained in (4.3) and must be specified by a boundary condition. By calculating the *strain rate* of the bulk, $\dot{\boldsymbol{\epsilon}}$, the corresponding bulk rotation can be found as

$$\boldsymbol{\omega}_b = \begin{bmatrix} 0 & 0 & \dot{\epsilon}_{13} \\ 0 & 0 & 0 \\ -\dot{\epsilon}_{13} & 0 & 0 \end{bmatrix} \tag{4.4}$$

The modelling of fabric in simple shear is thus more complicated than for the irrotational states. The lattice rotations are a combination of the usual migration towards the compressive axis and a right hand rotation about the y-axis resulting from the bulk rotation. Modelled simple shear fabrics are shown in Figure 4.2. The Lister model is unable to maintain a vertical fabric in simple shear; instead the fabric tilts to the axis of compression oriented at an angle of 45° to vertical. This result was also obtained by van der Veen and Whillans (1994) using an implementation of Sachs' and Lister's models. An alternate approach was taken by Azuma[1] (1994), applying the Schmid-Boas model, even though it is only formulated for uniaxial stress states. The rotation model was applied similar to uniaxial compression, i.e. individual grains rotate at the rate

$$\boldsymbol{\omega}_C = \dot{\epsilon}_{13} - 2\sin^2 \chi_c \dot{\gamma}_{(g)} \mathbf{S}^{(a)}_{(g)} \tag{4.5}$$

[1] In his article it is stated he uses the Lister model. This is a mistake and, in fact, the Schmid-Boas model was applied (Azuma, personal communication)

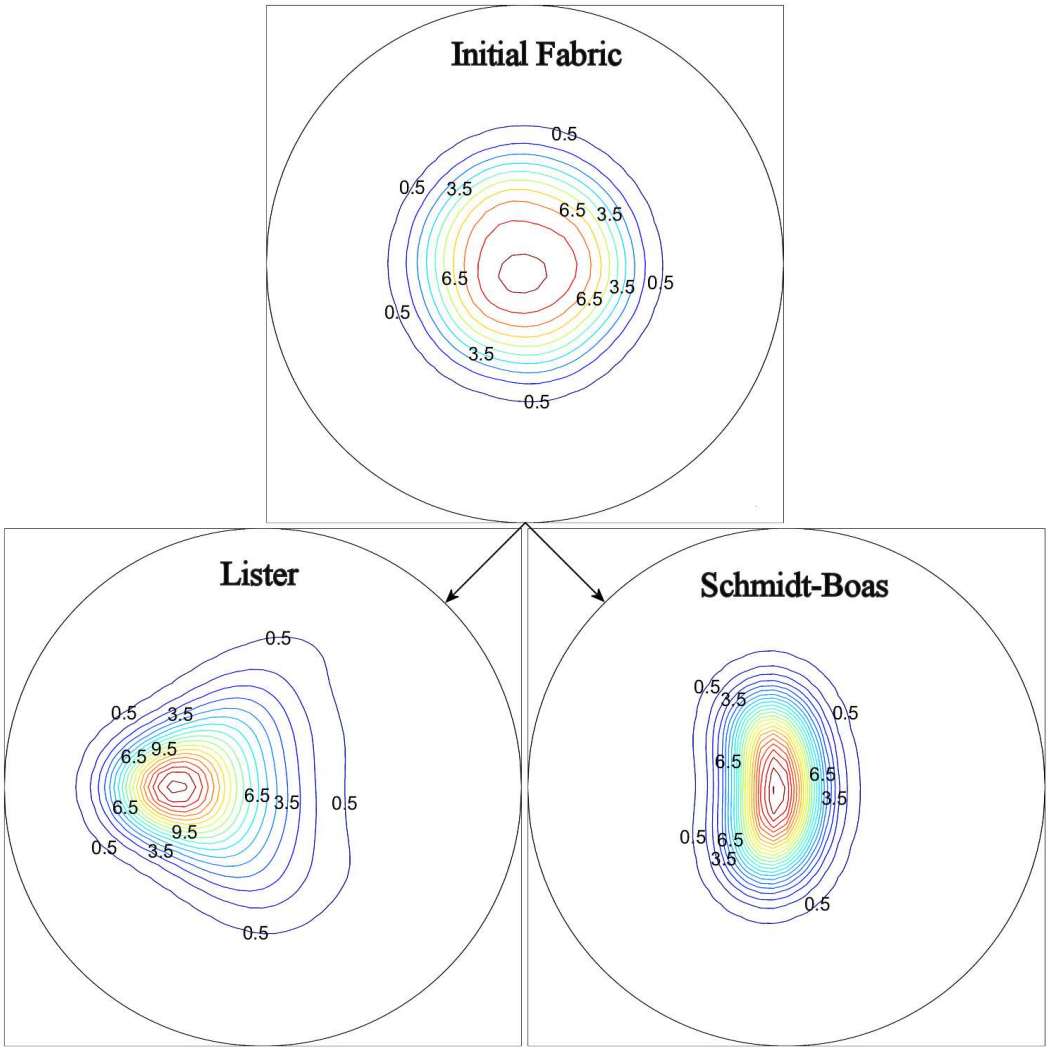

Figure 4.2: *Modelled fabric from simple shear deformation ($\epsilon_{xz} = 0.8$) using Azuma's model and either the Lister rotation model (left) or the Schmid-Boas model (right). The initial vertical fabric tilts towards the axis of compression when applying the Lister model, whereas the Schmid-Boas model maintains the vertical fabric.*

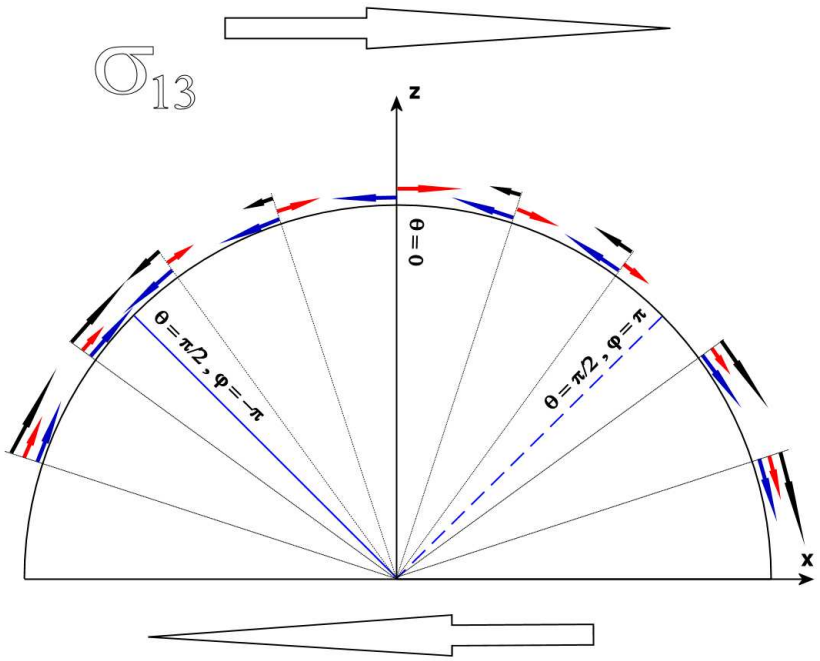

Figure 4.3: *The tilting of fabric in simple shear of the xz-plane using the Lister model. The rotation of individual c-axes are shown as a function of initial orientation. When a grain undergoes the shear displacement, γ_g, its c-axis will rotate, $\gamma_g/2$, towards the axis of compression (blue arrows). The boundary condition of simple shear implies the bulk rotation $\epsilon_{xz} = \langle S_g \gamma_g \rangle \leqq \langle \gamma_g \rangle /2$, where S_g is the Schmidt factor of the grain in respect to the axis of compression (the contribution to the bulk rotation by individual grains are shown by the red arrows). A single maximum fabric thus undergoes the rotation indicated by the black arrows. Vertical single maximum fabric is only a saddlepoint for the evolution, and even a single non-vertical grain will tilt the fabric towards the axis of compression. This is likely an artefact of the Lister model.*

where χ_c is the angle between the c-axis of the grain and the axis of compression. The Schmid-Boas models maintain the vertical fabric.

In the deep ice, where deformation is mainly simple shear, vertical fabric is observed, suggesting a problem with the Lister model, see Figure 4.3. It was proposed by van der Veen and Whillans (1994) that the vertical fabric could still be generated my migration recrystallization. Grains are expected to recrystallize at orientations favored for flow, i.e. along the x- and z-axes [Alley, 1992], which has also been confirmed in laboratory experiments. With a high rate of recrystallization the tilting of fabric could potentially be hindered by the formation of vertically orientated grains, although the accompanying formation of horizontally orientated grains made it very difficult to model.
In the community it is commonly accepted that the flow induced result of simple shear is vertical fabric, e.g. [Alley, 1992, Paterson, 1994], and it should be noted that this result can only be modelled with the Schmid-Boas model.

4.3 Simulating GRIP Fabric

The GRIP site is located on the Summit of the Greenland ice sheet. The local topography and measurements of surface strains are shown in Figure 4.4a. Ice is seen to stream radially away from the Summit, which is a roughly circular dome. In order to test the anisotropic flow models, the stress field at GRIP needs to be examined. The internal stress cannot be directly observed, though it can in principle be found by solving the stress equilibrium equations (3.22) along with the equation of continuity (3.28), a constitutive relation for ice and suitable boundary conditions for the surface, namely no shear stress along the ice surface and no stress normal to it. This problem reduces to seven equations with seven unknowns, meaning that the stress cannot be determined without assuming a constitutive relation. Of course it makes no sense to test the flow-prediction of

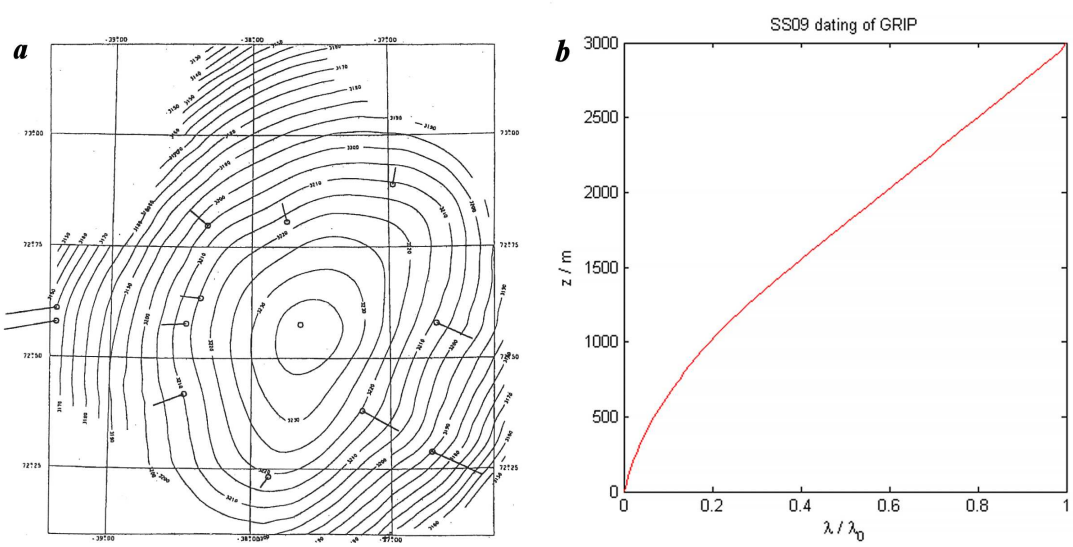

Figure 4.4: **a***: The surface topography at GRIP (equidistance* $5\,m$*). Vectors show surface velocity as measured between 1993-94 [Keller et al., 1995].* **b***: The strain-depth relation from the ss09 dating (Dansgaard-Johnsen model with* $h = 1500\,m$ *and* $FB = 0.135$*) [Johnsen et al., 1997].*

the anisotropic law against stresses predicted by Glen's law, since the idea is to improve it. At NorthGRIP Dahl-Jensen found the internal stresses using Azuma's model as the constitutive relation and Monte Carlo inversion(unpublished). Fabric was specified, from observations, as a function of depth, and fabric evolution was not modelled. Although this could be done at GRIP, it poses no *test* on Azuma's model.

This work is not concerned with the anisotropic models' ability to serve as a constitutive relation (though this is of course important) but rather with its ability to predict the evolution of fabric. By looking at fabric evolution separately, the problem of determining the *stress history* explicitly is avoided. In Lister's model, fabric depends only on deformation, while in Schmid-Boas' model it also depends on the *form*[2] of the stress deviator tensor. Ideally, the shear stress un-

[2]By the form $\mathbf{F}$, of a tensor $\mathbf{T}$, is meant $\mathbf{F} = \mathbf{T}/M$, where M is a scalar termed the *magnitude* of $\mathbf{T}$, such that $tr(\mathbf{F}^2) = 1$.

der the Summit will vanish due to the symmetry, so uniaxial compressive stress, with unknown magnitude dependent on depth and time, persists throughout the ice core. Even though the accumulation varies in time the vertical strain rate is, according to the Dansgaard-Johnsen model, a function of depth only, since there is no basal melt at GRIP. The relation between the thinning and depth at GRIP is shown in Figure 4.4b. Fabric evolution at GRIP can then be modelled as follows:

1. Initial fabric is chosen.
2. Fabric evolution and accumulated vertical strain is modelled with the anisotropic models, using a stress tensor corresponding to uniaxial compression with arbitrary magnitude.
3. Relating the accumulated vertical strain to the depth through the Dansgaard-Johnsen model, the fabric can be put on a depth scale and be compared to observations on the GRIP core.

This constitutes a very good test on the models' capabilities to describe fabric evolution, as the flow constant and thereby also temperature can be included in the arbitrary magnitude of stress. This means that the models contain no tuning parameters and no reconstruction of past accumulations, temperatures or stress fields is required.

4.3.1 Initial Fabric

The model will be run using two different initial conditions:

1. From the surface with isotropic initial fabric.
2. From a depth of $115\,m$ with polar angles distributed similar to observations at NorthGRIP by Svensson et al. (2003b) and randomly distributed azimuth angles, see Figure 4.5.

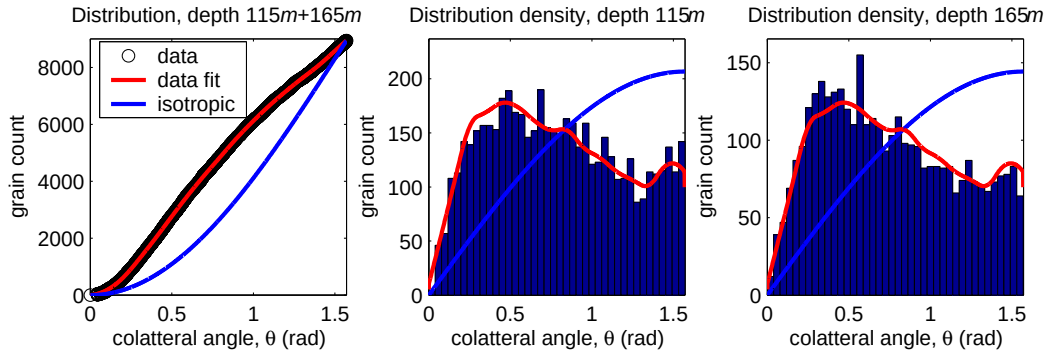

Figure 4.5: *Observed grain angles near the surface in the NorthGRIP core, data from Svensson et al. (2003b).* **Left***: (Cumulative) Distribution of polar angles (angle to vertical) measured on two thin sections from depth* $115\,m$ *and* $165\,m$ *(black circles), smooth fit to data (red line) and isotropic distribution (blue line). The fitted curve is used to generate non-isotropic initial fabric.* **Middle** *and* **Right***: Corresponding distribution densities along with histograms of observed polar angles from depth* $115\,m$ *and* $165\,m$ *respectively.*

4.3.2 Results

The results from the modelling of GRIP fabric is shown in Figure 4.6 with isotropic initial fabric. For reference the Sachs' flow model is also applied. The results of each of the four combinations of the two flow laws, Sachs' and Azuma, with the two rotation laws, Lister and Schmid-Boas, are plotted along with the observed fabric. Sachs' model predicts a slightly faster evolution of the degree of orientation. However, every combination predicts a too strong orientation below a depth around $500 - 900\,m$.

The model run with slightly anisotropic initial fabric determined from observations at NorthGRIP is shown in Figure 4.7. Again all combinations predict a too fast evolution of favored orientation, this time already from the top (depth $115\,m$). I introduce a correction to the Schmid-Boas rotation model reducing the individual grain rotations, as predicted from their strain, to 35% (This model is referred to as the *reduced Schmid-Boas model* in the following). The run using

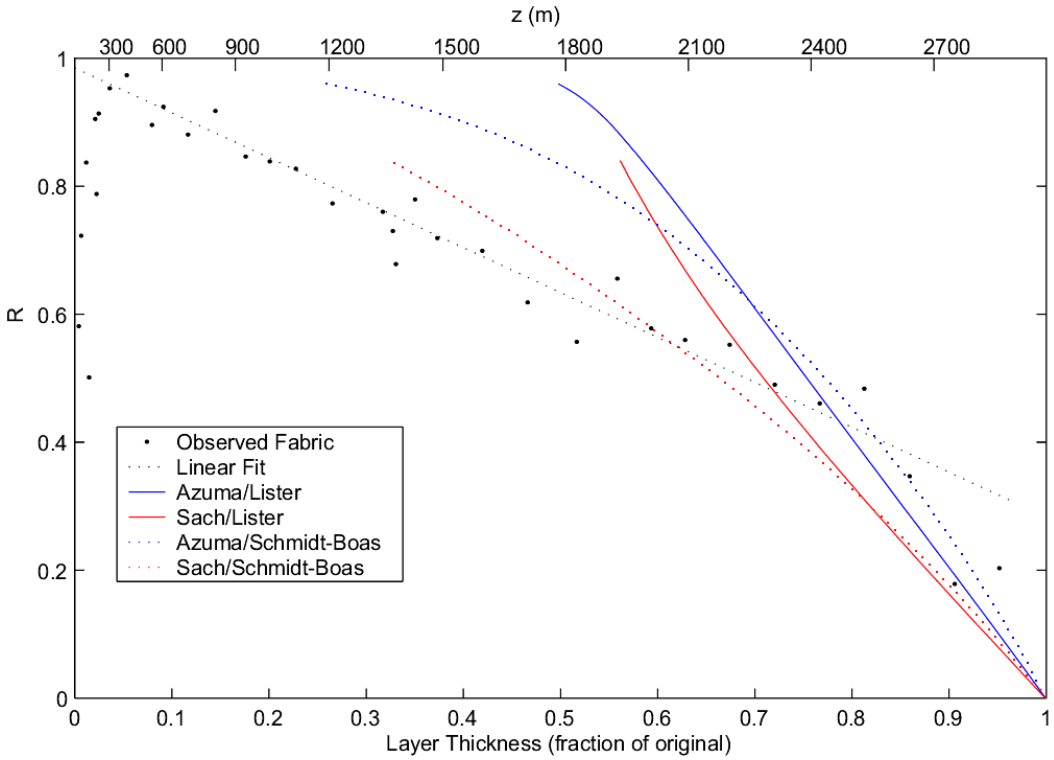

Figure 4.6: *Fabric evolution at GRIP, isotropic initial surface fabric. Four runs of the model using the different combinations of the two flow models and the two rotation models are shown. The evolution of fabric is modelled as a function of bulk vertical strain rate, and related to height above bedrock through the Dansgaard-Johnsen model. The observed values of R are calculated from the observations by Thorsteinsson et al. (1996). The models fit observations rather poorly, possibly with the exception of the Sachs/Schmid-Boas model. This model combination, however, produces a very unrealistic fabric, see Figure 4.9 for example.*

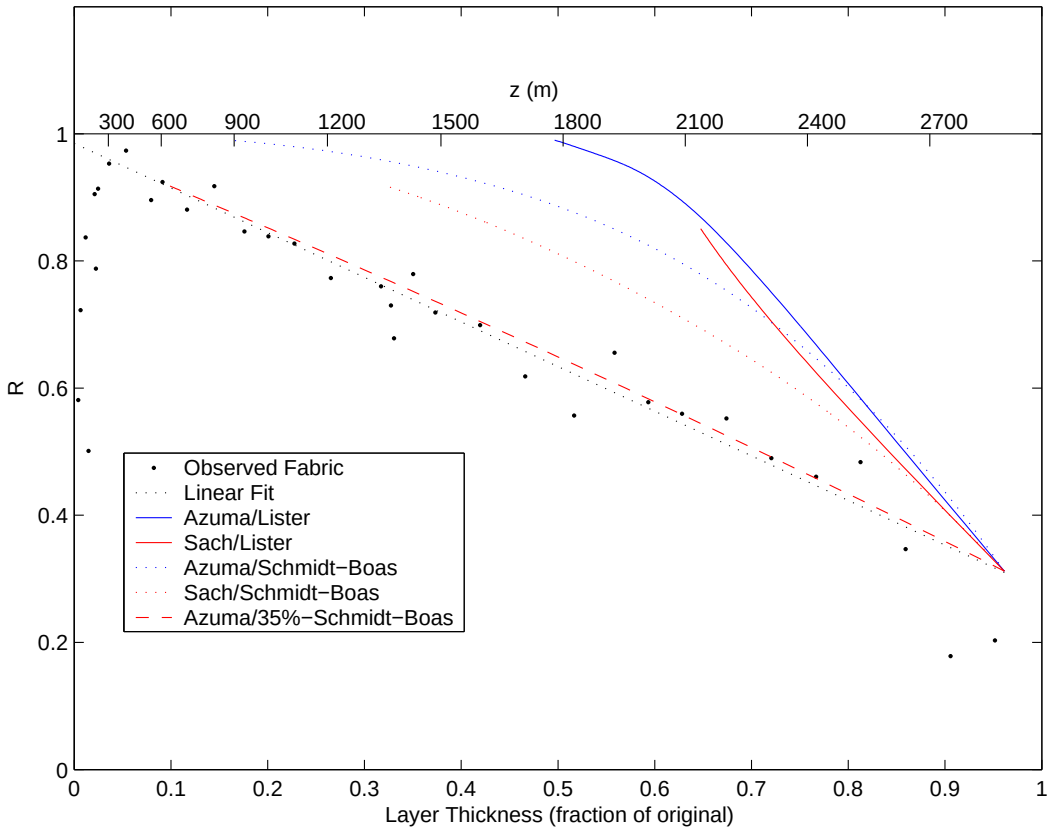

Figure 4.7: *Fabric evolution at GRIP, anisotropic firn ice transition. Also see text of Figure 4.6. All model runs predict fabric evolution, corresponding to grains rotating 2-3 times too fast (pr. vertical strain), compared to the observed fabrics. Though no theoretical justification is given, the Azuma/Schmid-Boas model can be fitted to data by reducing the grain rotations to 35% of the predicted (red dashed line).*

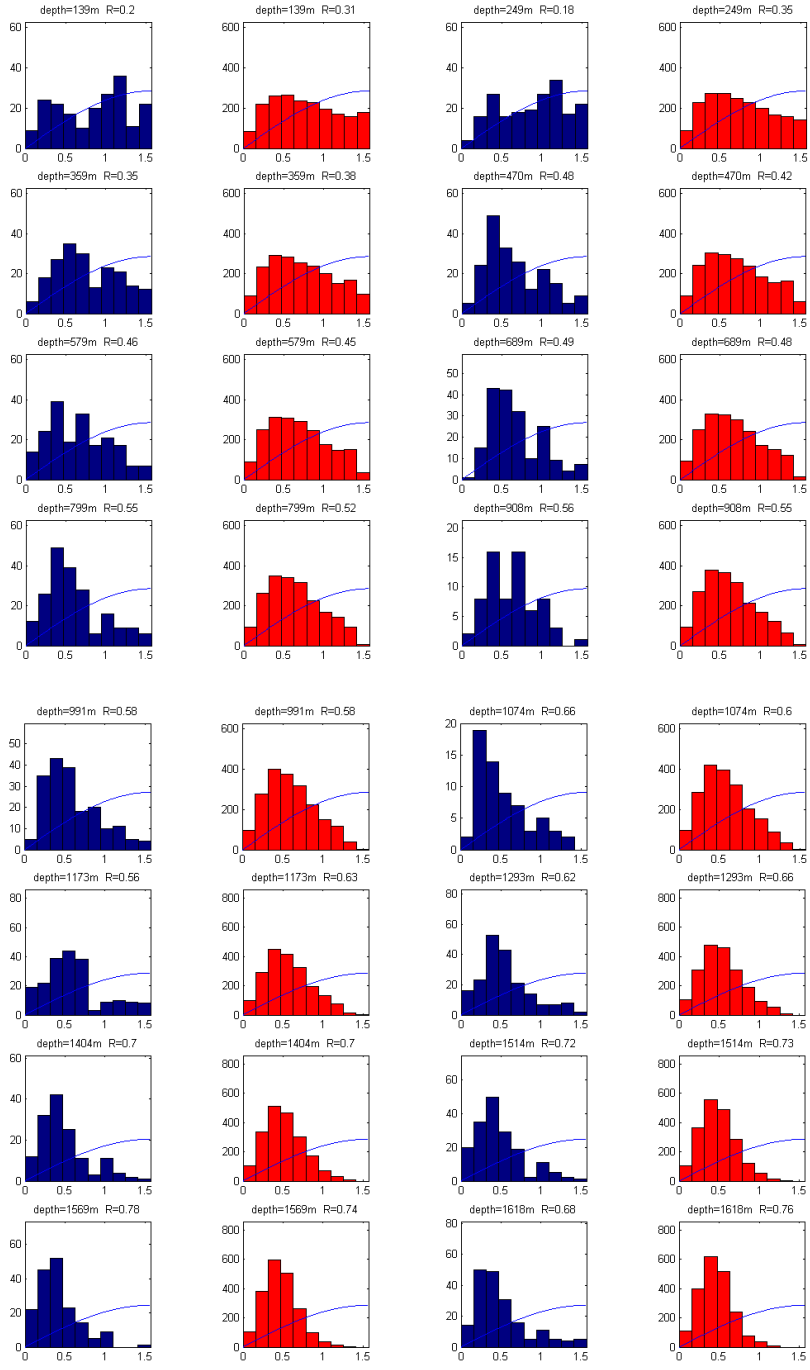
depth=139m R=0.2
depth=139m R=0.31
depth=249m R=0.18
depth=249m R=0.35
depth=359m R=0.35
depth=359m R=0.38
depth=470m R=0.48
depth=470m R=0.42
depth=579m R=0.46
depth=579m R=0.45
depth=689m R=0.49
depth=689m R=0.48
depth=799m R=0.55
depth=799m R=0.52
depth=908m R=0.56
depth=908m R=0.55
depth=991m R=0.58
depth=991m R=0.58
depth=1074m R=0.66
depth=1074m R=0.6
depth=1173m R=0.56
depth=1173m R=0.63
depth=1293m R=0.62
depth=1293m R=0.66
depth=1404m R=0.7
depth=1404m R=0.7
depth=1514m R=0.72
depth=1514m R=0.73
depth=1569m R=0.78
depth=1569m R=0.74
depth=1618m R=0.68
depth=1618m R=0.76

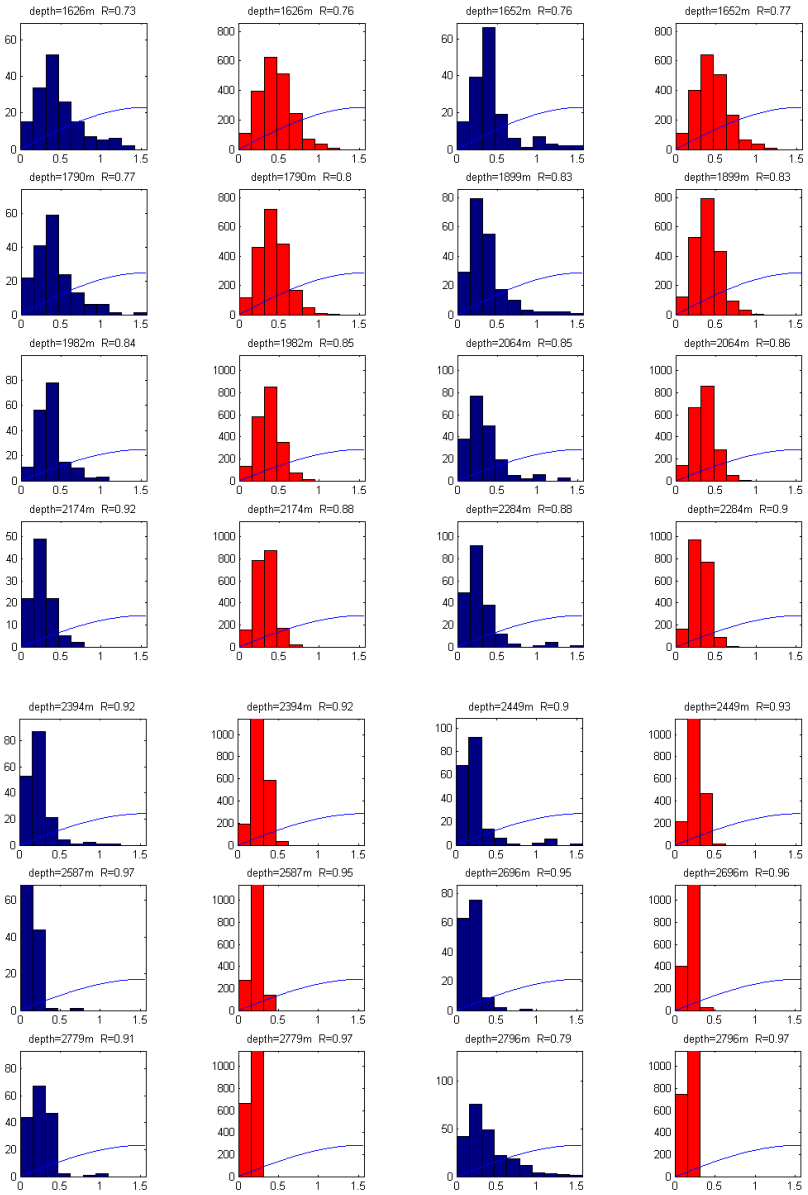

Figure 4.8: *Histograms of polar grain angles, θ, from observation from GRIP (blue) [Thorsteinsson et al., 1997] and from the Azuma/reduced Schmid-Boas model (red). The curve shows the isotropic orientation density. The modelled data are modelled using Azuma's flow model and a grain rotation equal to 35% of Schmid-Boas rotation model. The fabrics are circular, i.e. independent of azimuth angle. These histograms thus show the essential features of the fabric, demonstrating that the reduced Schmid-Boas model manages to produce very realistic fabrics without the inclusion of recrystallization models.*

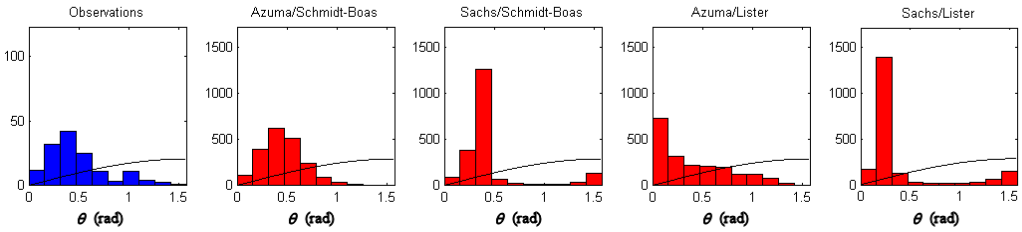

Figure 4.9: *Histograms of polar grain angles, θ, of fabric with $R = 0.73$ from observations at GRIP and from modelling. The Azuma/Schmid-Boas is seen to produce the most* realistic *distribution.*

this model, in combination with Azuma's model, is also plotted, fitting observations until 300 m above bedrock. The value of 35% is only chosen to fit the data; however it must be stressed that no other combination of the models presented here, can be fitted this way.

The degree of orientation or the eigenvalues (a_1, a_2, a_3) represent the fabric by simple numbers, making these measures useful, but neither fully characterize the anisotropic properties of the ice. Instead histograms of polar angles of individual grains give clear and full information, because of the circular fabric at GRIP. Figure 4.8 shows such histograms for the observed fabric vs. the modelled, using the reduced Azuma/Schmid-Boas model and anisotropic initial fabric. The modelled grain angle distribution fits remarkably well, considering the unjustified change to the rotation model. For comparison Figure 4.9 shows the orientation histograms of the other model combinations corresponding to $R = 0.73$. Only the Azuma/Schmid-Boas is seen to predict realistic fabric.

4.3.3 Discussion

As already discussed newer observations of near surface fabrics from NorthGRIP, which has surface conditions similar to GRIP, suggest that surface fabric is, in fact, far from isotropic. If this is true, the anisotropic models presented in this

work exaggerate the evolution of fabric already near the surface by $\sim 185\%$[3]. The strain-depth scale is very reliable in the Holocene, so one of two conclusions must be drawn:

1. Either, some process or combination of processes, already active near the surface, slow down the fabric evolution.

2. Or, the Lister and the Schmid-Boas rotation models both fail to correctly quantify the flow induced evolution of fabric. At least in combination with Sachs' and Azuma's model.

Even though the reduced Schmid-Boas model was tuned to match the upper fabric evolution, it predicts the fabric remarkably well until $z = 300\,m$. It is unclear whether this model predicts the true flow induced lattice rotations of the grains or whether it also contains the effects of other processes, i.e. dynamic recrystallization. For now, the reduced Schmid-Boas model is ignored, whilst possible processes slowing down the fabric evolution are examined.

4.3.4 Processes Reducing the Evolution of Fabric

Earlier investigations of the fabric evolution at GRIP using anisotropic models are all based on the assumption that ice is isotropic near the surface [Castelnau et al., 1996b, Thorsteinsson, 2002][4]. Castelnau et al., investigated the fabric evolution using a viscoplastic self-consistent model and came to the conclusion, in agreement with the models presented here, that modelled fabrics evolve too fast below $650\,m$ depth. This discrepancy was attributed to onset of rotation recrystallization at this depth. Thorsteinsson modelled the fabric using a new flow model, the mild

[3] $(1/0.35 - 1) * 100\%$

[4] Although, (Throstur) Thorsteinsson did note, based on the observations from GRIP, that surface fabric was slightly anisotropic

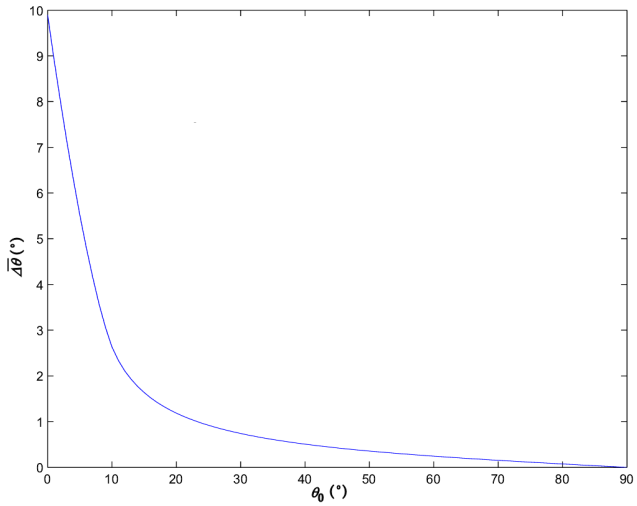

Figure 4.10: *Curve shows the expected mean change in polar angle, $\Delta\theta$, when a grain of initial angle, θ_0, is perturbed an angle of $\alpha = 10^o$ in a random direction, based on a calculation. In ice, subgrain boundaries are expected to form at angles $2\alpha < 15^o$ [Poirier, 1985]. The rotation of grains associated with rotation recrystallization is thus seen not to greatly affect orientation in average except when $\theta < 10^o$. Although in theory, rotation recrystallization could still indirectly affect the fabric through changes to the texture, see text.*

nearest neighbor interaction (NNI)[5] coupled to Listers rotation model. Rotation recrystallization was included in the model and the model fitted data from GRIP at depth 689 m and 1293 m in terms of distributions of polar angles. *Hard* grains were allowed to recrystallize, by breaking in two, provided their dislocation density, which was tracked for every grain, was above a critical value. Only one of the two new grains was retained in the model and it was assumed to rotate the polar angle $\pm\Delta\theta = 5^o$, but always away from vertical if $\theta < 30^o$. Though it is understandable that nearly vertical grains suffering a random rotation in average will rotate away from vertical, this implementation seems to exaggerate the effect, see Figure 4.10. Indeed a study, by this author, combining this scheme with the models presented in this work, could not reproduce these results, when the direction of rotation was instead chosen at random. Furthermore the total amount of recrystallization events necessary to match the observations is unspecified, even though a simple calculation shows that each grain must divide roughly every 2000 years in order to explain the stagnation observed in grain growth at this depth[Castelnau et al., 1996b], and a comparison with this value would have provided a useful test.
In summary, it is concluded that the mechanisms proposed here are unlikely to slow down fabric evolution sufficiently to account for the difference between the models and observations; especially near the surface, since it cannot significantly affect the orientation, except of nearly vertical grains ($\theta < 10^o$).

It cannot be ruled out that rotation recrystallization could affect fabric in combination with other processes. For instance by breaking hard grains, thereby making them susceptible for removal by normal grain growth. It is even possible that normal grain growth by itself could slow down fabric evolution by preferential growing of softer grains. As the time scales of grain-boundary migration

[5]Mild NNI can be shown to predict individual grain deformation almost equal to the average of the predictions of Azuma's and Sachs' model.

in the normal grain growth regime are expected to be long, a relation between grain size and orientation would be expected. A study of near surface texture and fabric at NorthGRIP, measuring 34119 grains, found no such relationship [Svensson et al., 2003b]. This suggests normal grain growth is not affecting fabrics, unless the hard grains are removed on short time-scales.

Migration recrystallization could potentially accommodate removal of hard grains on short time scales. A model was tested in which grains were assigned a probability proportional to their strain to recrystallize at 45° to vertical; however in order to match the near surface fabric evolution, so many recrystallization events were required that it became impossible to generate the high degree of orientation observed in the deeper core. Furthermore, several authors agree that migration recrystallization is not active at temperatures below $\sim -12^oC$, e.g. [Castelnau et al., 1996b], much warmer than the mean surface temperature of -32^o at GRIP [Johnsen et al., 1992]. It is very likely that the observed low degree of orientation, near the warmer bottom of the core, is the result of migration recrystallization, which is not accounted for by the models presented in this work.

Conclusions

Since no satisfactory process explaining the large discrepancy between the fabric evolutions modelled and observed was found, I propose the hypothesis that the reduced Schmid-Boas model represent the *real* flow induced lattice rotation, since it accounts for the observed fabric from the surface to the onset of the migration recrystallization regime at $z \sim 400\,m$. This proposal is theoretically unfounded and it can be difficult to visualize the constraints it places on the lattice rotations, but it could be tried as follows: Grains deform by simple shear of basal planes as seen from the *macroscopic* frame of reference, except the implied rotation is counteracted by a reduced (to 35% of the required value) compensating

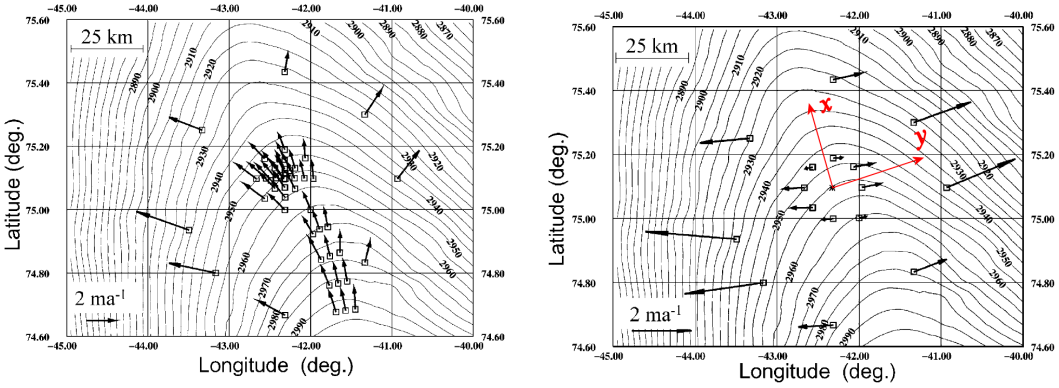

Figure 4.11: *The surface topography at NorthGRIP (located in the center), equidistance* 5 *m and definition of the frame of reference used. Left: Surface velocity, as measured at 44 stakes (see scale). Right: Surface velocity relative to the drill site (only 16 stakes shown). As seen, the surface is strained normal to the ridge. Figures from Hvidberg et al. (2002).*

lattice rotation acting to keep horizontal material lines from rotating. A non-zero vorticity for deforming grains is implied, which is also the case for the original Schmid-Boas model. This is not a theoretical problem as the required moments of force could be supplied by the neighboring grains. Regardless of the lack of elegance contained in this rotation model, it still deserves to be tested elsewhere, based solely on its nice reproduction of data. Unfortunately, it is not clear how to extend, even the original Schmid-Boas model, to a general stress configuration. Nevertheless, it will be tested on NorthGRIP using the very simple extension already described in Section 4.2.2.

4.4 Simulating NorthGRIP Fabric

It is more difficult to model the fabric evolution at NorthGRIP. Unlike GRIP, NorthGRIP is not situated on a dome, complicating the stress field. Furthermore upstream effects and the presence of basal melt makes it difficult to relate the vertical strain to depth. These problems will be addressed in the following.

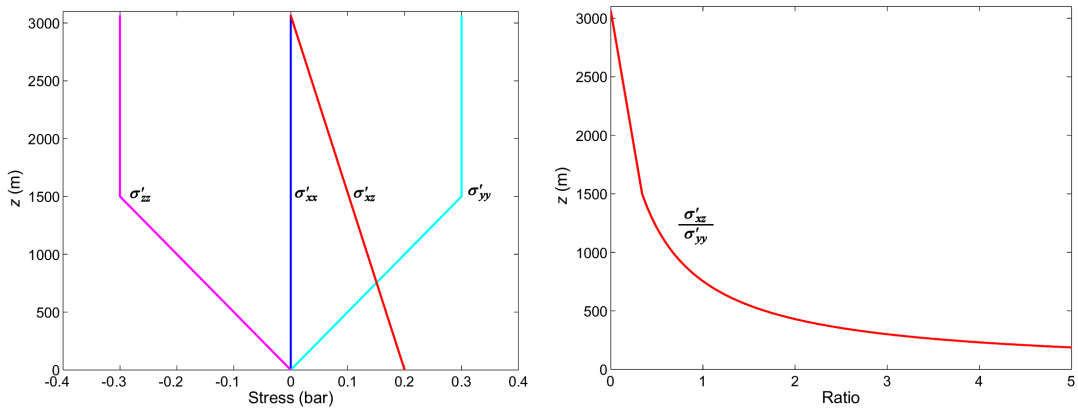

Figure 4.12: **Left**: *Schematic presentation of relation between z and components of stress tensor at NorthGRIP as modelled by Dahl-Jensen. The pure shear is constant for $z > 1500\,m$ decreasing linearly to zero below. The simple shear, σ_{xz} is zero at the surface increasing linearly with depth.* **Right**: *The ratio of simple shear to pure shear, $r(z)$, used to determine the form of the stress tensor .*

NorthGRIP is located on the northwestern ridge of the Greenland ice sheet where the ice thickness is $3085\,m$ (roughly $3065\,ice\,equiv.\,m$). Define the x-axis to be horizontal along the ridge and the y-axis to be horizontal normal to the x-axis, see Figure 4.11. Ice flows from the Summit along the ridge past NorthGRIP in the x-direction. The velocities relative to the NorthGRIP site are almost orthogonal to the ridge corresponding to a surface strain along the ridge of only $\dot{\epsilon}_{xx} = (-0.4 \pm 0.6) \times 10^{-5} a^{-1}$ compared to $\dot{\epsilon}_{yy} = (7.1 \pm 0.6) \times 10^{-5} a^{-1}$ across [Hvidberg et al., 2002]. As mentioned, Dahl-Jensen found the present day stress field schematically shown in Figure 4.12, based on these boundary conditions and Azuma's model. Pure shear is dominant in the upper ice sheet, with extensive axis along the y-axis. Simple shear of the xz-plane, caused by basal drag, develops with depth. At the ridge, simple shear of the yz-plane will entirely vanish (in theory), due to the symmetry.

The Dansgaard-Johnsen model can be applied along a flow line parallel to y, although the flow line will be translated along the x-axis. For these calculations

upstream effects, i.e. the spatial dependance of accumulation and the model parameters, $H(x)$, $h(x)$ etc., are ignored. The steady state predictions of the model using present-day accumulation will exaggerate the thinning of annual layers in the Wisconsin ice because the accumulation in this period was lower. This estimate can be improved by numerically integrating (3.18) using the accumulation history derived from $\delta^{18}O$ [Andersen et al., 2004]. By integrating from different start times the present accumulated thinning of original layers can be reconstructed, see Figure 4.13. When applying the anisotropic model, the ratio of pure shear to simple shear, $r(z) = \sigma_{xz}(z)/\sigma_{yy}(z)$, is required. $r(z)$ is determined at each time step by relating the modelled accumulated vertical strain to z through the *present-day* thinning relation. Naturally the present-day thinning-depth relation is not valid before present, however the error made is probably small compared to the unknown time dependance of σ_{xz}/σ_{yy}. The models can then be run similar to the GRIP simulation, bearing in mind that the *form* of the stress deviator must be continuously updated. The form of the Cauchy stress deviator is thus

$$\boldsymbol{\sigma}'(z) = \begin{bmatrix} 0 & 0 & r(z) \\ 0 & 1 & 0 \\ r(z) & 0 & -1 \end{bmatrix} \tag{4.6}$$

Initial fabric is chosen matching observations [Svensson et al., 2003b], see Figure 4.5, and the model is started at depth $115\,m$. Only the Azuma model combined with the reduced Lister model will be applied. It is easily verified that the form of the stress deviator (4.6) implies the presence of one compressive and two extensive principal stress axes at all depths. The simple form (4.5) for the Schmid-Boas rotation is used.

4.4.1 Results

Only the Azuma/reduced Schmid-Boas model was applied to the NorthGRIP conditions. The modelled fabric eigenvalues are displayed in Figure 4.14. For

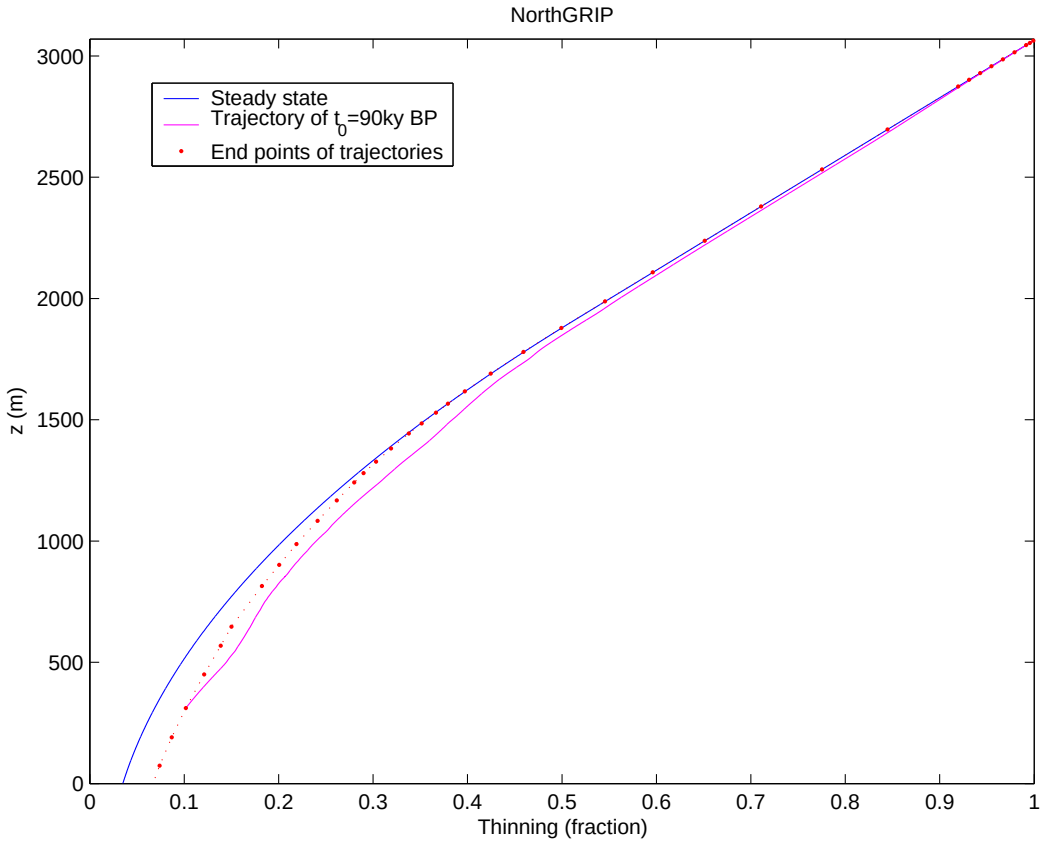

Figure 4.13: *The relationship between vertical thinning of annual layers and height above bedrock as predicted by the Dansgaard-Johnsen model. Because basal melting is occurring at NorthGRIP, the thinning of any annual ice layer depends on the accumulation history following the deposition. Blue line shows the thinning assuming accumulation is constant in time. Red dots show the present day thinning when accumulation history is taken into account. Magenta line, shows an example of calculation of present-day thinning. The thickness of a layer deposited on the surface* $90ky\,BP$ *is found by numerical integration of the first equality of* (3.16) *forward in time and space.*

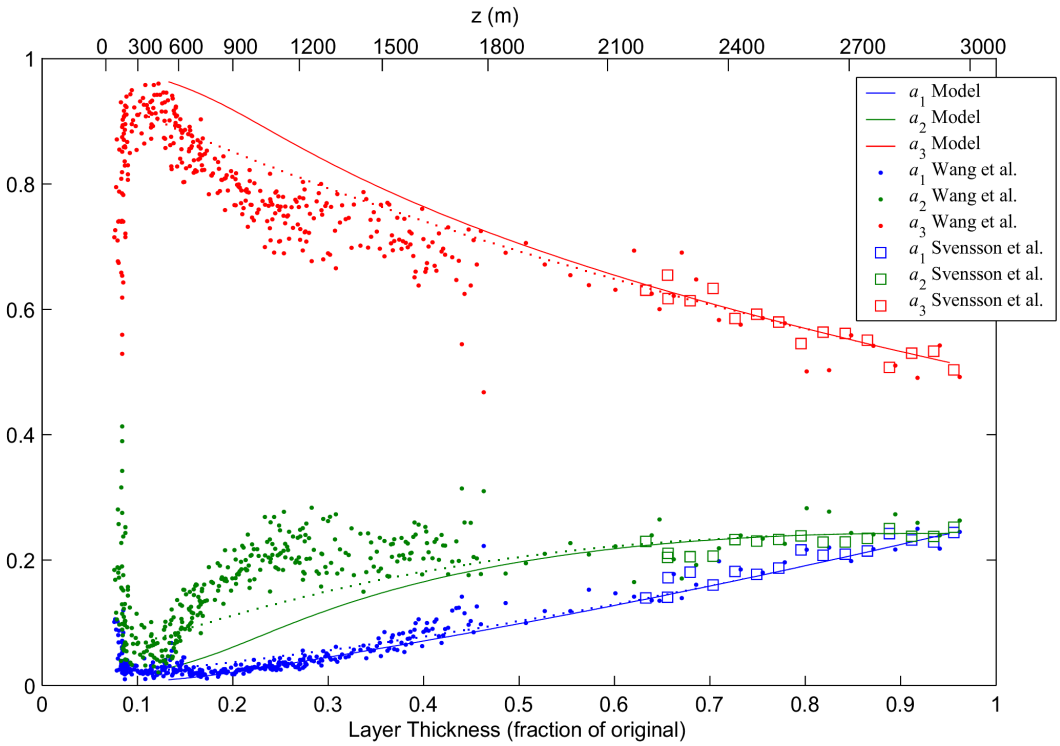

Figure 4.14: *Fabric evolution at NorthGRIP, modelled from anisotropic firn ice transition. The eigenvalues of the observed fabric is shown as dots and boxes. Modelled fabric is shown as solid lines and the dotted line shows a model-run without simple shear. The model shows a very good agreement with observations until* $z \sim 1700\,m$*. At this depth a slight kink in the observed fabric evolution is seen. Hence even the model-run without simple shear exaggerates vertical fabric evolution, below this point, suggesting that either the simple shear reduces fabric evolution, or some effects not accounted for have disturbed the fabric or depth-strain scale.*

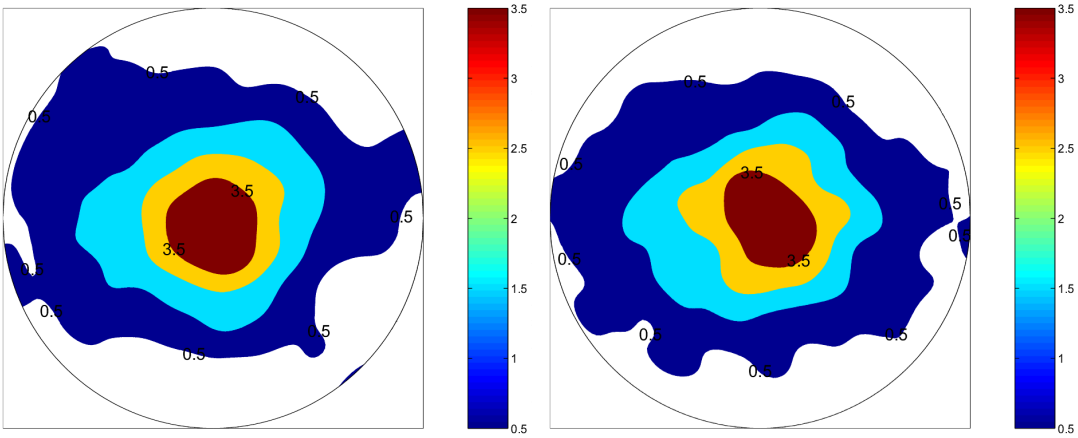

Figure 4.15: **Left**: *Contoured orientation plot of observed orientations of* 1910 *grains from NorthGRIP, depth* 605 *m* (*z* = 2480 *m*) *[Svensson et al., 2003b].* **Right**: *Corresponding modelled orientations of* 4000 *grains.*

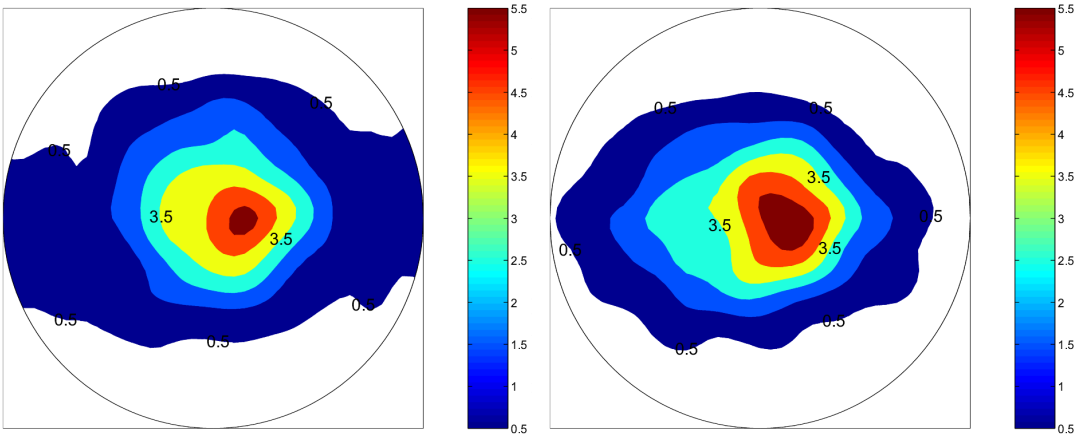

Figure 4.16: **Left**: *Contoured orientation plot of observed orientations of* 1591 *grains from NorthGRIP, depth* 880 *m* (*z* = 2205 *m*) *[Svensson et al., 2003b].* **Right**: *Corresponding modelled orientations of* 4000 *grains.*

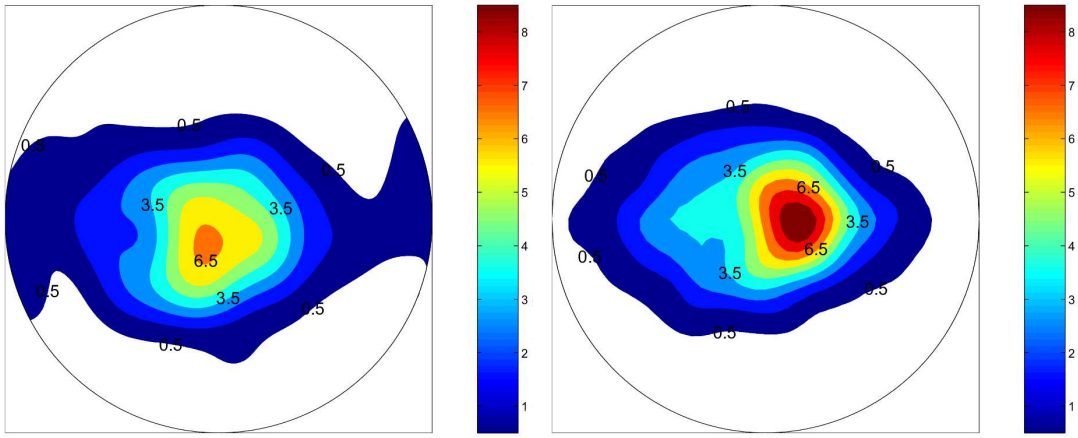

Figure 4.17: Left: *Contoured orientation plot of observed orientations of* 202 *grains from NorthGRIP, depth* 1328 *m* ($z = 1757\,m$)*[Wang et al., 2002].* **Right**: *Corresponding modelled orientations of* 2000 *grains.*

comparison, the model was also run without simple shear, as shown by the dotted curves. The results are in very good agreement with observations above $z \sim 1700\,m$, even matching the formation of the girdle fabric, i.e. the separation of a_1 and a_2. Below this point the model exaggerates the rate of formation of vertical fabric. The inclusion of simple shear can be seen to further increase the modelled strength of orientation.

The developing asymmetrical fabric reduces the usefulness of the histograms of polar grain angles shown for GRIP data. Figure 4.15, 4.16 and 4.17 show Schmidt contour plots of modelled fabrics compared to the observed at depth $605\,m$ and $880\,m$ respectively. These also show good agreement. It has unfortunately been impossible to obtain the raw data files containing observed c-axis orientations from NorthGRIP between a depth of $880\,m$ and $1328\,m$, so Schmidt plots from these intervals cannot be compared.[6]

[6]This constitutes the brittle ice zone which was measured later. These datafiles have apparently been misplaced.

4.4.2 Discussion

The reduced Azuma/Schmid-Boas model is seen to handle remarkably well, at least until $z \sim 1700\,m$, just above the climatic transition. A decrease in the observed rate of vertical fabric evolution (a_3) on the strain scale is seen at this depth, which is not found in the modelled evolution. Several possible interpretations of the deviation below this point could be made. Errors in the depth-thinning scale could produce incorrect representation of observed data, or errors in the form of the stress deviators could put the model off. Alternatively the model fails to correctly predict the fabric caused by simple shear. Finally a change in impurity content across the transition could influence the fabric evolution, although no similar effect is observed in the GRIP core.

The upstream effects can be difficult to assess because it requires knowledge of the spatial and temporal dependence of the Dansgaard-Johnsen model parameters. Based on the observed surface velocity of $1.30\,ma^{-1}$, a simple calculation shows that ice from the climatic transition ($z \sim 1600\,m$, age 11703 years b2k) originates only $\sim 15\,km$ upstream, suggesting the discrepancy can not solely be excused by upstream effects. Probably the time dependance of the model parameters could provide a larger effect. The climatic transition is likely accompanied by a change in the model parameters which would modify the thinning-depth relationship, although the extent of this modification is constrained by the good agreement between the Dansgaard-Johnsen model and the stratigraphic dating. It is concluded that errors on the thinning-depth relation cannot account for the discrepancy between modelled and observed fabrics.

The used form of the stress tensor is only valid under present-day conditions. Lower glacial accumulation likely leads to a different surface topography changing σ_{yy}/σ_{xz}. Furthermore, even a small migration of the ice ridge in the y-direction

could imply a strong simple shear of the yz-plane. In the model, horizontal simple shear increases the evolution of vertical fabric; hence the model-run without simple shear can somewhat be considered a lower bound for the evolution of a_3. Since even this run overestimates the evolution of vertical fabric, it is very unlikely that any change to σ_{xz}/σ_{yy} or even the inclusion of σ_{yz} in the stress deviator could account for the discrepancy below $z \sim 1700\,m$, unless the simple shear actually *reduces* the evolution of vertical fabric. Longitudinal tensions along the ridge would reduce the fabric evolution, and would also explain the high degree of girdle fabric observed at high depth; however, at $z \sim 1700\,m$ such tensions cannot arise from bedrock undulations, especially since the bedrock is very flat near NorthGRIP [Dahl-Jensen et al., 1997].

A satisfactory explanation of the discrepancy below $z \sim 1700\,m$ was not found. Even though the Azums/35%-Schmid-Boas represents an ad hoc fit to the evolution of R at GRIP, its reproduction of NorthGRIP Holocene and GRIP orientation densities grants a certain degree of fidelity to the model, at least for the irrotational stress states. Its capabilities to predict fabrics formed under simple shear remain untested.

To the knowledge of this author, no prior investigations of the fabric evolution at NorthGRIP have been performed allowing no comparisons of these results.

Chapter 5

Summary and Conclusions

Previous attempts to determine fabric evolution in ice sheets by application of anisotropic models, are based on the interpretation of observations that near surface ice has random orientation. This has led to the conclusion that anisotropic models were in good agreement with observations of fabric in the upper $\sim 700\,m$ of the GRIP core, at which depth the onset of rotation recrystallization was thought to slow down the evolution of vertical fabric. With the introduction of automated fabric analyzers, measurements with better statistics revealed moderately anisotropic ice already in the upper layers at other sites, although some uncertainty still persists whether this holds true at GRIP.

In this work, a setup of Azuma's and Sachs' model in combinations with Lister's and Schmid-Boas' has been presented. It has been demonstrated that the corrections to initial fabrics implies an overestimation of the lattice rotations of individual grains by $\sim 185\%$ at GRIP and NorthGRIP, already near the surface, by these anisotropic models. Furthermore the Lister model produces unrealistic fabric containing too many hard grains, and it is unable to maintain vertical fabric under simple shear deformation.

A change to the Schmid-Boas lattice rotation has been proposed, reducing lattice rotations to 35%. In combination with Azuma's model it reproduced the fabric at GRIP from the surface to $300\,m$ above bedrock, without the inclusion of a separate model for rotation recrystallization. Below this depth observed fabric has reduced orientation, which very likely can be attributed to migration recrystallization due to the high temperature or possibly to folding and rotation of layers. It is unclear how to extend the Schmid-Boas model from the uniaxial stress states to a general stress state. A simple extension was performed and the reduced Schmid-Boas model was applied at NorthGRIP, closely matching observations to above $z \sim 1700\,m$, corresponding to a depth of $\sim 1400\,m$. At this depth the simple shear is beginning to affect the deformation. It was argued that the discrepancy below this depth was probably not due to the model's inability to handle simple shear; rather it might be the result of increased concentrations of impurities in the Wisconsin ice or inclusion of more components in the stress tensor. Sadly, the Azuma/reduced Schmid-Boas model thus remains untested in its ability to model realistic fabrics resulting from simple shear. In ice sheets, ice mainly deforms by simple shear, except near the ice divides, elevating the need for a detailed understanding of its effect on the fabric.

Despite the problems in the lower parts of the NorthGRIP core, the Azuma/reduced Schmid-Boas model shows a good potential. This suggests that the evolution fabric is mainly determined by ice flow, except when the temperature is close to the melting point, where migration recrystallization is important. No conclusions on the effects of impurity contents can be drawn based on this work. Further tests of the Azuma/reduced Schmid-Boas model is required, especially in simple shear zones. Only then can usefulness of the model be evaluated. Tests of the capabilities of Azuma's model as a constitutive relation for ice, under deformation at the low stresses observed in ice sheets, must also be made.

5.1 Further Work

It is important to know the initial fabric on the GRIP core. It will be relatively easy to measure the fabrics of a few thin sections close to the firn-ice transition using the automatic *c*-axis analyzer at the Niels Bohr Institute, once and for all settling the issue.

As argued in this work, the flow induced evolution of fabric should be independent of accumulation and temperature, as long as there is no basal melt and migration recrystallization does not occur. This should be tested by comparing the reduced Schmid-Boas model to the fabric observations performed on the Dome C ice core in Antarctica by Wang et al. (2003). Here the ice flow is similar to GRIP as ice undergoes uniaxial compression and the temperature and accumulation is very different.

As mentioned, further testing of the reduced Schmid-Boas model under rotational stress states are required. To this end it would be interesting to compare the model to the fabrics of the DYE 3 core, although further measurements on the core would probably be required.

Appendix A

Statistic and Graphic Representation of Texture and Fabric

A.1 Statistics

A.1.1 Texture Parameters

Various shape parameters for individual ice crystals can be obtained automatically by analyzing digital images of the thin sections, [Wang and Azuma, 1999, Hansen, 2001].

Cross sectional area, A_{meas}, is usually the most important texture property of a crystal since it is related to crystal volume, V. Assuming crystals to be spherical, for instance, the best estimate for the volume is

$$< V >_{est} = \frac{4}{3}\left(\frac{3}{2}A_{meas}\right)^{3/2} \tag{A.1}$$

where the factor of 3/2 arises because the cross section is generally not at the equator of the crystals. Even though the expected mean grain volume is proportional to the 3/2 power of A_{meas}, the arithmetic mean of A_{meas} is usually employed to characterize the texture of a sample. Earlier studies have employed a plethora of measures for grain size making absolute comparison difficult (at best).

Other texture parameters include *width*, *height*, *flattening* (ratio of width to

height) and *roundness* (ratio of circumference of grain to ellipse of same area and flattening). Grains are often flattened in the vertical direction, due to compressive straining. Assuming grains to ellipsoid, the mean flattening of vertical thin sections can be used to refine (A.1).

A.1.2 Fabric Parameters

Thin sections of ice sheet ice typically contain several hundreds of grains. To compare the fabric of different thin sections, some statistical parameters characterizing the strength of orientation in a sample must be chosen. Several simple parameters have often been employed, e.g. the half apex-angle of a cone containing 90% of the c-axes, the spherical aperture and many more. Throughout this work, two measures are adopted, R the degree of orientation and the eigenvalues a_1, a_2, a_3 of the cross-product tensor $\mathbf{a}^{(2)}$.

The degree of orientation, originally introduced by Wallbrecher (1978), is defined as

$$R = \frac{2S - N}{N} \quad , \quad \text{where} \quad S = \frac{1}{N} \left| \sum_{i}^{N} \mathbf{c}_i \right| \tag{A.2}$$

S is called the *normalized length of the resultant vector*, N is the number of grains in the sample and $\mathbf{c}_i$ is the Cartesian c-axis vector of grain i. R is zero for isotropic fabric, increasing to one for completely uniform orientation, while R can also be negative. c-axes have no inherent up and down. It is therefore implicitly assumed that the frame of reference is chosen such that *up* is along the *best axis of symmetry* (evaluated using either a least square method [Durand et al., 2006a] or common sense), and that the sign of every c-axis is chosen such that it points *up*. It is a theoretical weakness of R that its value depends on the choice of the c-vector sign, so care must be taken in the computation. In practice, however, the *best axis of symmetry* is usually vertical. I will occasionally use R, primarily justified by it's simplicity, describing the fabric by a single number.

The eigenvalues, a_1, a_2, a_3, of the cross-product tensor

$$\mathbf{a}^{(2)} = \sum_{i=1}^{N} f_i \mathbf{c}_i \otimes \mathbf{c}_i \tag{A.3}$$

yields more information of the fabric. f_i is the weight of crystal i. Weighting each grain the same

$$f_i = 1/N \tag{A.4}$$

alternatively weighting the orientation of each grain by its volume yields

$$f_i = \frac{A_i^{3/2}}{\sum_{j=1}^{N} A_j^{3/2}} \tag{A.5}$$

where A_i is the observed cross sectional area of grain i, assuming grain *shape* is independent of size. It is reasonable to weigh orientations by grain size, as larger crystals effect the properties of the polycrystal more than smaller ones, but information of grain sizes is not always available. Since studies have found no correlation between grain size and orientation [Svensson et al., 2003b], the choice of weighing is not important. The eigenvectors of $\mathbf{a}^{(2)}$ can be interpreted as three orthonormal vectors along the axes of the ellipsoid best fitting the distribution of c-axes, while the corresponding eigenvalue represent the length of each axis [Woodcock, 1977]. The eigenvalues satisfy the equation

$$a_1 + a_2 + a_3 = 1 \tag{A.6}$$

A.2 Plotting Fabric

In this section it is discussed how to graphically represent a set of c-axes. Traditionally each crystal has been plotted as a dot in a Schmidt plot; however when more than a few c-axes are plotted the Schmidt plot is difficult to interpret, i.e. dots become indistinguishable. To avoid this problem data are sometimes presented as a (2D) histogram. Finally a new continuous method of plotting inspired by the work of Throstur Thorsteinsson is described.

A.2.1 The Schmidt Plot

The c-axis of a ice crystal can be regarded as a point on a unit hemisphere and is described by the azimuthal angle ϕ and the zenith angle θ. In order to map a c-axis a projection from the hemisphere to the plane is thus required. Traditionally the Lambert azimuthal projection, known from geodesy, is used

$$\begin{aligned} (\theta, \phi) &\rightarrow (r(\theta), \phi) \\ r(\theta) &= sin\frac{\theta}{2} \end{aligned} \tag{A.7}$$

This is also an equal area projection thereby ensuring that the dots in a map of an isotropic sample will be evenly distributed. This mapping of a set of c-axes is known as a *Schmidt plot*.

A.2.2 Orientation Density

A measured set of c-axes at one point in the ice should be regarded as a sample of an underlying distribution, since the goal is to obtain information about fabric in the ice surrounding the point not just in the point itself. It is very hard to infer from the dotted Schmidt plots whether any clustering and other features have any statistical significance. Increasing the sample size will of course reduce the statistical fluctuations, but this only raises the problem that dotted Schmidt plots becomes cluttered and unreadable.

Kamb (1959) addressed this problem by dividing the Schmidt plot into bins of fractional area A and counting the crystals in each. He then plotted contours of orientation-density instead of individual data points. The idea was to construct a robust graphical representation of data, i.e. one that only showed preferred orientations statistically significant. The statistical significance of the observed orientation-density is measured by the probability of making a similar sample from a truly isotropic distribution. Kamb therefore adjusted A for a given N as follows:

Sampling N orientations and dividing them into bins can be considered a multinomial experiment. Assuming that the unknown underlying distribution is isotropic then the expected number of crystals in each bin, E, and standard deviation thereof, σ, will be equal in every bin and given by

$$E = NA \tag{A.8}$$

$$\sigma^2 = NA(1 - A) \tag{A.9}$$

To ensure that individual samples will not fluctuate wildly the bin area is chosen such that $E/\sigma = 3$, using (A.8) and (A.9) this yields

$$A = \frac{9}{N + 9} \tag{A.10}$$

Observed data are then contoured in intervals of 2σ. Bin counts of 3σ correspond to isotropic orientation density while for instance the 4σ-contour borders orientations preferred at significance level σ, etc. This is indeed the great strength of Kamb's plots, namely that statistical significance of any apparent structure in the fabric can be directly seen on the plot. The fidelity of preferred orientations is further increased when preferred direction bins are adjacent. Often contour plots are presented computed from a bin area much smaller than given by (A.10), showing details not sufficiently supported by the observations. In fact a very large sample size is required to make high resolution plots, eg. for 100 bins 891 crystals are required.

A.2.3 Continuous Plots

While Kamb's contour plots indeed yield robust results, an objection to it is that by dividing orientations into bins the method does not utilize all the information of the sample. A continuous method of making orientation-density plot is therefore presented. In line with the reasoning of Kamb the goal is still to estimate the *true* orientation probability distribution, $\hat{G}(\mathbf{c})$, in ice surrounding the

sample. Assuming a smooth underlying probability density distribution, each observed orientation yields information about $\hat{G}$, also for *nearby* orientations.

Considering a sample $\{\mathbf{c}_1, \mathbf{c}_2, ..., \mathbf{c}_N\}$ of size N. An estimate $G(\mathbf{c})$ of $\hat{G}(\mathbf{c})$ is constructed as a superposition of N small normal distributions, $g_i(c)$, each centered on a data point.

$$G(\mathbf{c}) = \frac{1}{N} \sum_{i=1}^{N} g_i(\mathbf{c}) \tag{A.11}$$

$$g_i(\mathbf{c}) = k \exp\left(\frac{-1}{s^2}(\mathrm{dist}(\mathbf{c}, \mathbf{c}_i)^2)\right) \tag{A.12}$$

The angular difference between two orientations is taken as their distance. Since ice crystals have no *up* or *down* direction angles cannot exceed $\pi/2$ and can be calculated as

$$\mathrm{dist}(\mathbf{c}_i, \mathbf{c}_j) \equiv \min\{\angle(\mathbf{c}_i, \mathbf{c}_j), \angle(-\mathbf{c}_i, \mathbf{c}_j)\} = \cos^{-1}(|\mathbf{c}_i \cdot \mathbf{c}_j|) \tag{A.13}$$

k is the normalization constant such that the area integral of each $g_i(c)$ over a hemisphere is equal to one

$$\frac{1}{k} = 2\pi \int_0^{\pi/2} \exp\left(\frac{-\theta^2}{s^2}\right) \sin\theta d\theta \tag{A.14}$$

s is a measure of the width of the small distributions. $G(\mathbf{c})$ can then be contoured in a Schmidt diagram by applying the mapping (A.7). Searching for a robust estimate $G(\mathbf{c})$, s must be adjusted by the number of c-axes sampled. Picking s too large will smooth any structure in $G(\mathbf{c})$ whereas a too small value will show insignificant features; indeed in the limit $s \to 0$ the classical dotted Schmidt plot is obtained. Loosely speaking, each crystal then gives information about the fractional area (when $s << \frac{\pi}{2}$)

$$A = \frac{\pi s^2}{2\pi} = \frac{s^2}{2} \tag{A.15}$$

In the line of Kamb, one can somewhat loosely argue that each data point should

yield information of a fractional area given by (A.10). Inserting (A.15) yields

$$s = \frac{\alpha}{\sqrt{9+N}} \tag{A.16}$$

$$\alpha = 2\sqrt{3} \tag{A.17}$$

The value of α should not be taken too seriously as the definition of the area covered by g_i could be chosen otherwise. (A.16) however shows how s should scale with N, once a value of α is decided.

Appendix B

Distribution of Stress in Azuma's Model

Uniaxial Compression

The classic Schmid-Boas formula for the evolution of polar angle, θ, of individual grains during vertical compression is

$$\sin\theta = \sin\theta_0\,(1 + \Delta\epsilon_g) \tag{B.1}$$

where θ_0 is the initial angle before the vertical strain on the grain, $\Delta\epsilon_g$. The goal of this section is to rewrite (B.1) as a relation between small rotation angles, $d\theta$, and small basal shear displacements, $d\gamma$. To this end, (B.1) is rearranged

$$\sin\theta - \sin\theta_0 = \Delta\epsilon_g \sin\theta_0 \tag{B.2}$$

Using a standard trigonometric identity and the definition $\Delta\theta = \theta - \theta_0$, the left hand side of (B.2) can be rewritten as

$$\begin{aligned}\sin\theta - \sin\theta_0 &= 2\cos\frac{\theta+\theta_0}{2} \cdot \sin\frac{\theta-\theta_0}{2} \\ &= 2\cos(\theta_0 + \frac{\Delta\theta}{2})\sin\frac{\Delta\theta}{2}\end{aligned} \tag{B.3}$$

For small values of $\Delta\theta$ (B.3) becomes

$$\sin\theta - \sin\theta_0 = \cos\theta_0 \cdot \frac{d\theta}{2} \tag{B.4}$$

Recall that the relation between a small vertical strain $d\epsilon_g$ and basal shear $d\gamma_g$ of an individual grain is

$$d\epsilon_g = S_g d\gamma_g = \sin\theta_0 \cos\theta_0 d\gamma_g \tag{B.5}$$

Inserting (B.4) and (B.5) in (B.2) and dividing by $\cos\theta_0$, the final result is obtained

$$d\theta = 2\sin^2\theta \, d\gamma \tag{B.6}$$

QED.

Uniaxial Extension

It can be shown in the same manner that the formula for crystal rotation during uniaxial extension

$$\cos\theta = \cos\theta_0 \left(1 + \Delta\epsilon_g\right)^{-1} \tag{B.7}$$

is equivalent to the angle differential

$$d\theta = 2\cos^2\theta \, d\gamma \tag{B.8}$$

Bibliography

[Alley et al., 1986] Alley, R., Perepezko, J., and Bentley, C. (1986). Grain growth in polar ice: Ii. application. *Journal of Glaciology*, 32(112):425–433.

[Alley, 1992] Alley, R. B. (1992). Flow-law hypotheses for ice-sheet modelling. *Journal of Glaciology*, 38(129):245–256.

[Alley and Woods, 1996] Alley, R. B. and Woods, G. A. (1996). Impurity influence on normal grain growth in the GISP2 ice core, Greenland. *Journal of Glaciology*, 42(129):255–260.

[Andersen et al., 2004] Andersen, K. K., Azuma, N., Barnola, J.-M., Bigler, M., Biscaye, P., Caillon, N., Chappellaz, J., Clausen, H. B., Dahl-Jensen, D., Fischer, H., Flckiger, J., Fritzsche, D., Fujii, Y., Goto-Azuma, K., Grœnvold, K., Gundestrup, N. S., Hansson, M., Huber, C., Hvidberg, C. S., Johnsen, S. J., Jonsell, U., Jouzel, J., Kipfstuhl, S., Landais, A., Leuenberger, M., Lorrain, R., Masson-Delmotte, V., Miller, H., Motoyama, H., Narita, H., Popp, T., Rasmussen, S. O., Raynaud, D., Rothlisberger, R., Ruth, U., Samyn, D., Schwander, J., Shoji, H., Siggaard-Andersen, M.-L., Steffensen, J. P., Stocker, T., Sveinbjörnsdóttir, A. E., Svensson, A., Takata, M., Tison, J.-L., Thorsteinsson, T., Watanabe, O., Wilhelms, F., and White, J. C. (2004). High-resolution record of northern hemisphere climate extending into the last interglacial period. *Nature*, 431:147–151.

[Azuma, 1994] Azuma, N. (1994). A flow law for anisotropic ice and its application to ice sheets. *Earth and Planetary Science Letters*, 128:601–614.

[Azuma, 1995] Azuma, N. (1995). A flow law for anisotropic polycrystalline ice under uniaxial compressive deformation. *Cold Regions Science and Technology*, 23:137–147.

[Azuma and Higashi, 1985] Azuma, N. and Higashi, A. (1985). Formation processes of ice fabric pattern in ice sheets. *Annals of Glaciology*, 6:130–134.

[Bishop and Hill, 1951] Bishop, J. and Hill, R. (1951). A theory of plastic distortion of a polycrystalline aggregate under combined stress. *Philos. Mag.*, 42:414–427.

[Bizet, 2006] Bizet, B. (2006). High resolution analysis of the microstructures and fabrics of the ice from the NGRIP ice core: A detailed study of 3 D.O. events (1,8,19). Master's thesis, Ice and Climate, Niels Bohr Institute for Astronomy, Physics, and Geophysics, University of Copenhagen, Denmark. Title may change.

[Castelnau et al., 1996a] Castelnau, O., Duval, P., Lebensohn, R. A., and Canova, G. R. (1996a). Viscoplastic modeling of texture development in polycrystalline ice with a self-consistent approach; comparison with bound estimates. *Journal of Geophysical Research*, 101(B6):13,851–13,868.

[Castelnau et al., 1996b] Castelnau, O., Thorsteinsson, T., Kipfstuhl, J., Duval, P., and Canova, G. R. (1996b). Modelling fabric development along the grip ice core central greenland. *Annals of Glaciology*, 23:194–201.

[Dahl-Jensen, 1989] Dahl-Jensen, D. (1989). Steady thermomechanical flow along two-dimensional low lines in large grounded ice sheets. *Journal of Geophysical Research*, 94(B8):10355–10362.

[Dahl-Jensen and Gundestrup, 1987] Dahl-Jensen, D. and Gundestrup, N. S. (1987). Constitutive properties of ice at dye 3, greenland. *The Physical Basis of Ice Sheet Modelling*, (170):31–43.

[Dahl-Jensen et al., 2003] Dahl-Jensen, D., Gundestrup, N. S., Gogineni, P., and Miller, H. (2003). Basal melt at NorthGRIP modeled from borehole, ice-core and radio-echo sounder observations. *Annals of Glaciology*, 37:207–212.

[Dahl-Jensen et al., 1997] Dahl-Jensen, D., Gundestrup, N. S., Keller, K., Johnsen, S. J., Gogeneni, P., Allen, C. T., Chuah, T. S., Miller, H., Kipfstuhl, S., and Waddington, E. D. (1997). A search in north Greenland for a new ice-core drill site. *Journal of Glaciology*, 43(144):300–306.

[Dansgaard, 1964] Dansgaard, W. (1964). Stable isotopes in precipitation. *Tellus*, 16(4):436–468.

[Dansgaard and Johnsen, 1969] Dansgaard, W. and Johnsen, S. J. (1969). A flow model and a time scale for the ice core from Camp Century, Greenland. *Journal of Glaciology*, 8(53):215–223.

[Diprinzio et al., 2005] Diprinzio, C. L., Wilen, L. A., Alley, R. B., Fitzpatrick, J. J., Spencer, M. K., and Gow, A. J. (2005). Fabric and texture at Siple Dome, Antarctica. *Journal of Glaciology*, 51(173):281–290.

[Durand et al., 2006a] Durand, G., Gagliardini, O., Thorsteinsson, T., Svensson, A., Kipfstuhl, J., and Dahl-Jensen, D. (2006a). Ice microstructure and fabric: an up to date approach to measure textures. *Submitted to Journal of Glaciology*.

[Durand et al., 2006b] Durand, G., Weiss, J., Lipenkov, V., Delmonte, B., Röthlisberger, R., and Bigler, M. (in press, 2006b). Effect of impurities on grain growth in cold ice sheets. *Journal of Geophysical Research*.

[Duval et al., 1983] Duval, P., Ashby, M., and Anderman, I. (1983). Rate-controlling processes in the creep of polycrystalline ice. *J. Phys. Chem.*, 87:4066–4074.

[Ganopolski and Rahmstorf, 2001] Ganopolski, A. and Rahmstorf, S. (2001). Stability and variability of the thermohaline circulation in the past and future: A study with a coupled model of intermediate complexity. In Seidov, D., Maslin, M., and Haupt, B. J., editors, *The Oceans and Rapid Climate Change: Past, Present and Future*, pages 261–275. AGU, Washington.

[Glen, 1955] Glen, J. (1955). The creep of polycrystalline. volume Ser. A , 228 (1175), pages 519–538. Proc. R. Soc. London.

[GRIP Members, 1993] GRIP Members (1993). Climate instability during the last interglacial period recorded in the grip ice core. *Nature*, 364(6434):203–208.

[Hansen, 2001] Hansen, K. M. (2001). Textures and fabrics of ice crystals in the GRIP ice core – A detailed study of glacial interstadial 3. Master's thesis, Department of Geophysics, Niels Bohr Institute for Astronomy, Physics, and Geophysics, University of Copenhagen, Denmark.

[Hvidberg et al., 2002] Hvidberg, C. S., Keller, K., and Gundestrup, N. S. (2002). Mass balance and ice flow along the north-northwest ridge of the Greenland ice sheet at NorthGRIP. *Annals of Glaciology*, 35:521–526.

[Jacka, 1984] Jacka, T. (1984). Laboratory studies on relationships between ice crystal size and flow rate. *Cold Regions Science and Technology*, 10:31–42.

[Johnsen et al., 1992] Johnsen, S., Clausen, H., Dansgaard, W., Fuhrer, K., Gundestrup, N., Hammer, C., Iversen, P., Steffensen, J., Jouzel, J., and Stauffer, B. (1992). Irregular glacial interstadials recorded in a new greenland ice core. *Nature*, 359(6393):311–313.

[Johnsen et al., 1997] Johnsen, S. J., Clausen, H. B., Dansgaard, W., Gundestrup, N. S., Hammer, C. U., Andersen, U., Andersen, K. K., Hvidberg, C. S., Dahl-Jensen, D., Steffensen, J. P., Shoji, H., Sveinbjörnsdóttir, A. E., White, J., Jouzel, J., and Fisher, D. (1997). The δ^{18}O record along the Greenland Ice Core Project deep ice core and the problem of possible Eemian climate instabillity. *Journal of Geophysical Research*, 102(C12):26397–26410.

[Johnsen et al., 1995] Johnsen, S. J., Dahl-Jensen, D., Dansgaard, W., and Gundestrup, N. (1995). Greenland palaeotemperatures derived from GRIP bore hole temperature and ice core isotope profiles. *Tellus*, 47B:624–629.

[Johnson, 1977] Johnson, A. F. (1977). Creep charecterization of transversely isotropic metallic materials. *J. Mech. Phys. Solids*, 25:117–126.

[Jun, 1995] Jun, L. (1995). *Interrelation between flow proporties and crystal structure of snow and ice*. PhD thesis, University of Melbourne.

[Kamb, 1959] Kamb, W. B. (1959). Ice petrofabric obeservations from Blue Glacier, Washington, in relation to theory and experiment. *Journal of Geophysical Research*, 64(11):1801–1909.

[Kamb, 1961] Kamb, W. B. (1961). The glide direction of ice. *Journal of Glaciology*, 3:1097–1106.

[Keller et al., 1995] Keller, K., Gundestrup, N., Dahl-Jensen, D., Tscherning, C. C., Forsberg, R., and Ekholm, S. (1995). The ice deformation and mass balance at the Summit of Greenland as determined by GPS and gravity measurements. In Obleitner, F. and Olesen, O., editors, *Mass Balance and Related Tropics of the Greenland Ice Sheet*, Open File Ser. 95/5, pages 15–18. Grœnlands Geol. Unders., Copenhagen, Denmark.

[Langway, 1958] Langway, Chester C., J. (1958). Ice fabrics and universal stage. *CRREL*, Technical Report 62:1–15.

[Lister et al., 1978] Lister, G. S., Paterson, M. S., and Hobbs, B. E. (1978). The simulation of fabric development in plastic deformation and its application to quarzite: The model. *Tectonophysics*, 45:107–158.

[Mathiesen et al., 2004] Mathiesen, J., Ferkinghoff-Borg, J., Jensen, M., Levinsen, M., Olesen, P., Dahl-Jensen, D., and Svensson, A. (2004). Dynamics of crystal formation in the greenland northgrip ice core. *Journal of Glaciology*, 50(170):325–328.

[Montagnat and Duval, 2000] Montagnat, M. and Duval, P. (2000). Rate controlling processes in the creep of polar ice, influence of grain boundary migration associated with recrystallization. *Earth and Planetary Science Letters*, 183:179–186.

[Nye, 1957] Nye, J. (1957). The creep of polycrystalline. volume Ser. A , 239 (1216), pages 113–133. Proc. R. Soc. London.

[Paterson, 1994] Paterson, W. S. B. (1994). *The Physics of Glaciers*. Pergamon Press, Oxford.

[Petrenko and Whitworth, 1999] Petrenko, V. F. and Whitworth, R. W. (1999). *Physics of Ice*. University Press, Oxford.

[Poirier, 1985] Poirier, J. P. (1985). *Creep of Crystals*. Cambridge University Press, New York.

[Rigsby, 1951] Rigsby, G. (1951). Crystal fabric studies on Emmons glacier, Mount Rainer, Washington. *J. Geology*, 49:590–598.

[Ruth et al., 2003] Ruth, U., Wagenbach, D., Steffensen, J. P., and Bigler, M. (2003). Continuous record of microparticle concentration and size distribution in the central greenland ngrip ice core during the last glacial period. *Journal of Geophysical Research*, 108(D3):4098, doi:10.1029/2002JD002376.

[Sachs, 1928] Sachs, G. (1928). Zur Ableitung einer Fliessbedingung. *Z. Ver. Dtsch. Ing.*, 72(103):734–736.

[Schmid and Boas, 1985] Schmid, E. and Boas, W. (1985). *Kristallplastizität.* Cambridge University Press, New York.

[Svensson et al., 2003a] Svensson, A., Baadsager, P., Persson, A., Hvidberg, C. S., and Siggaard-Andersen, M. (2003a). Seasonal variability in ice crystal properties at NorthGRIP: A case study around 301m depth. *Annals of Glaciology*, 37:119–122.

[Svensson et al., 2003b] Svensson, A., Schmidt, K. G., Dahl-Jensen, D., Johnsen, S. J., Wang, Y., Kipfstuhl, S., and Thorsteinsson, T. (2003b). Properties of ice crystals in NorthGRIP late - to middle-Holocene ice. *Annals of Glaciology*, 37:113–118.

[Thorsteinsson, 1996] Thorsteinsson, T. (1996). *Textures and fabrics in the GRIP ice core, in relation to climate history and ice deformation.* PhD thesis, Alfred-Wegener Institut Fr Polar- Und Meeresforchung.

[Thorsteinsson, 2002] Thorsteinsson, T. (2002). Fabric development with nearest-neighbor interaction and dynamic recrystallization. *Journal of Geophysical Research*, 107(B1):1–13.

[Thorsteinsson et al., 1997] Thorsteinsson, T., Kipfstuhl, J., and Miller, H. (1997). Texture and fabrics in the grip ice core. *Journal of Geophysical Research*, 102(C12):26,583–26,599.

[Thorsteinsson et al., 1999] Thorsteinsson, T., Waddington, E., Taylor, K., Alley, R., and Blankenship, D. (1999). Strain-rate enhancement at dye 3, greenland. *Journal of Glaciology*, 45(150):338345.

[van der Veen and Whillans, 1994] van der Veen, C. J. and Whillans, I. M. (1994). Development of fabric in ice. *Cold Regions Science and Technology*, 22:171–195.

[Vinther et al., 2006] Vinther, B., Clausen, H., Johnsen, S., Rasmussen, S., Andersen, K., Buchardt, S., Dahl-Jensen, D., Seierstad, I., Siggaard-Andersen, M.-L., Steffensen, J., Svensson, A., Olsen, J., and Heinemeier, J. (2006). A synchronized dating of three greenland ice cores throughout the holocene. *Journal of Geophysical Research*, page Doi:10.1029/2005JD006921.

[Wallbrecher, 1978] Wallbrecher, E. (1978). Ein cluster-verfahren zur richtungsstatistichen analyse tektonischer daten. *Geologische Rundschau*, 67:880–857.

[Wang and Azuma, 1999] Wang, Y. and Azuma, N. (1999). A new automatic ice-fabric analyzer which uses image analysis techniques. *Annals of Glaciology*, 29:155–162.

[Wang et al., 2003] Wang, Y., Kipfstuhl, J., Azuma, N., Thorsteinsson, T., and Miller, H. (2003). Ice-fabrics study in the upper 1500m of the Dome C (East Antarctica) deep ice core. *Annals of Glaciology*, 37:97–104.

[Wang et al., 2002] Wang, Y., Thorsteinsson, T., Kipfstuhl, J., Miller, H., Dahl-Jensen, D., and Shoji, H. (2002). A vertical girdle fabric in the northgrip deep ice core, north greenland. *Annals of Glaciology*, 35:515–520.

[Weertan, 1983] Weertan, J. (1983). Creep deformation of ice. *Annu. Rev. Earth Planet. Sci.*, 11:215–240.

[Wilen et al., 2003] Wilen, L. A., Diprenzio, C. L., Alley, R. B., and Azuma, N. (2003). Development, principles, and applications of automated ice fabric analyzers. *Microscopy resarch and technique*, 62:2–18.

[Woodcock, 1977] Woodcock, N. (1977). Specification of fabric shapes using an eigenvalue method. *Geol. Soc. Am. Bull.*, 88:1231–1236.